

RESEARCH PAPER



## Phosphorylation of KRT8 (keratin 8) by excessive mechanical load-activated PKN (protein kinase N) impairs autophagosome initiation and contributes to disc degeneration

Di Wang<sup>1</sup>, Qiliang Shang<sup>1</sup>, Jianxin Mao<sup>1</sup>, Chu Gao<sup>1,2</sup>, Jie Wang<sup>1</sup>, Dong Wang<sup>1</sup>, Han Wang<sup>1</sup>, Haoruo Jia<sup>1</sup>, Pandi Peng<sup>1,2</sup>, Mu Du<sup>1</sup>, Zhuojing Luo<sup>1,2</sup>, and Liu Yang<sup>1,2</sup>

<sup>1</sup>Institute of Orthopedic Surgery, Xijing Hospital, Fourth Military Medical University, Xi'an, People's Republic of China; <sup>2</sup>Medical Research Institute, Northwestern Polytechnical University, Xi'an, People's Republic of China

### ABSTRACT

Excessive mechanical load (overloading) is a well-documented pathogenetic factor for many mechano stress-induced pathologies, i.e. intervertebral disc degeneration (IDD). Under overloading, the balance between anabolism and catabolism within nucleus pulposus (NP) cells are badly thrown off, and NP cells undergo apoptosis. However, little is known about how the overloading is transduced to the NP cells and contributes to disc degeneration. The current study shows that conditional knockout of *Krt8* (keratin 8) within NP aggravates load-induced IDD in vivo, and overexpression of *Krt8* endows NP cells greater resistance to overloading-induced apoptosis and degeneration in vitro. Discovery-driven experiments shows that phosphorylation of KRT8 on Ser43 by overloading activated RHOA-PKN (protein kinase N) impedes trafficking of Golgi resident small GTPase RAB33B, suppresses the autophagosome initiation and contributes to IDD. Overexpression of *Krt8* and knockdown of *Pkn1* and *Pkn2*, at an early stage of IDD, ameliorates disc degeneration; yet only knockdown of *Pkn1* and *Pkn2*, when treated at late stage of IDD, shows a therapeutic effect. This study validates a protective role of *Krt8* during overloading-induced IDD and demonstrates that targeting overloading activation of PKNs could be a novel and effective approach to mechano stress-induced pathologies with a wider window of therapeutic opportunity.

**Abbreviations:** AAV: adeno-associated virus; AF: annulus fibrosus; ANOVA: analysis of variance; ATG: autophagy related; BSA: bovine serum albumin; cDNA: complementary deoxyribonucleic acid; CEP: cartilaginous endplates; CHX: cycloheximide; cKO: conditional knockout; Cor: coronal plane; CT: computed tomography; Cy: coccygeal vertebra; D: aspartic acid; DEG: differentially expressed gene; DHI: disc height index; DIBA: dot immunobinding assay; dUTP: 2'-deoxyuridine 5'-triphosphate; ECM: extracellular matrix; EDTA: ethylene diamine tetraacetic acid; ER: endoplasmic reticulum; FBS: fetal bovine serum; GAPDH: glyceraldehyde-3-phosphate dehydrogenase; GPS: group-based prediction system; GSEA: gene set enrichment analysis; GTP: guanosine triphosphate; HE: hematoxylin-eosin; HRP: horseradish peroxidase; IDD: intervertebral disc degeneration; IF: immunofluorescence staining; IL1: interleukin 1; IVD: intervertebral disc; KEGG: Kyoto encyclopedia of genes and genomes; KRT8: keratin 8; KD: knockdown; KO: knockout; L: lumbar vertebra; LBP: low back pain; LC/MS: liquid chromatograph mass spectrometer; LSI: mouse lumbar instability model; MAP1LC3/LC3: microtubule associated protein 1 light chain 3; MMP3: matrix metalloproteinase 3; MRI: nuclear magnetic resonance imaging; NC: negative control; NP: nucleus pulposus; PBS: phosphate-buffered saline; PE: p-phycoerythrin; PFA: paraformaldehyde; PI: propidium iodide; PKN: protein kinase N; OE: overexpression; PTM: post translational modification; PVDF: polyvinylidene fluoride; qPCR: quantitative reverse-transcriptase polymerase chain reaction; RHOA: ras homolog family member A; RIPA: radio immunoprecipitation assay; RNA: ribonucleic acid; ROS: reactive oxygen species; RT: room temperature; TCM: rat tail compression-induced IDD model; TCS: mouse tail suturing compressive model; S: serine; Sag: sagittal plane; SD rats: Sprague-Dawley rats; shRNA: short hairpin RNA; siRNA: small interfering RNA; SOFG: safranin O-fast green; SQSTM1: sequestosome 1; TUNEL: terminal deoxynucleotidyl transferase dUTP nick end labeling; VG/ml: viral genomes per milliliter; WCL: whole cell lysate.

### ARTICLE HISTORY

Received 11 December 2022

Revised 23 February 2023

Accepted 25 February 2023

### KEYWORDS

Autophagosome initiation; intervertebral disc degeneration; keratin 8; phosphorylation; Protein kinase N


### Introduction

Low back pain (LBP) is a commonly seen musculoskeletal disorder in people of all age [1,2]. The lifetime prevalence of LBP is nearly 80%, and it has been reported that about 1 in 4

adults in the USA had low back pain that lasted for at least 24 hours within the previous 3 months [3,4]. A growing body of evidence has established a causative link between IDD and low back pain [5].

**CONTACT** Zhuojing Luo [zjluo@fmmu.edu.cn](mailto:zjluo@fmmu.edu.cn)  Institute of Orthopedic Surgery, Xijing Hospital, Fourth Military Medical University, No. 169, Changle West Road, Xincheng District, Xi'an, Shaanxi Province, People's Republic of China; Liu Yang [yangliu@fmmu.edu.cn](mailto:yangliu@fmmu.edu.cn)  Institute of Orthopedic Surgery, Xijing Hospital, Fourth Military Medical University, No. 169, Changle West Road, Xincheng District, Xi'an, Shaanxi Province, People's Republic of China

<sup>†</sup>Di Wang, Qiliang Shang, Jianxin Mao, Chu Gao contributed equally to this work.

 Supplemental data for this article can be accessed online at <https://doi.org/10.1080/15548627.2023.2186099>

The intervertebral disc (IVD) is a fibrocartilaginous pad which is responsible for resisting spinal compression while permitting limited movements at the same time [6–8]. Three distinct yet interrelated structures constitute the IVD: the peripheral annulus fibrosus (AF); the cartilaginous endplates (CEP); and the central nucleus pulposus (NP), which is a gelatinous, tissue, rich in proteoglycans [9]. Healthy NP is a highly hydrated cushioning pad, which is capable of distributing the mechanical loading among the spine into the surrounding AF and the adjacent CEPs, appropriately. A degenerated NP is characterized by loss of proteoglycans, resulting in loss of water content within the NP [10]. Hence, the capacity of loading cushioning and distribution of NP would be largely compromised [11].

To date, various causes have been linked to the development of IDD, including genetic pre-disposition, aging, obesity, heavy labor, etc [12]. Accumulative evidence has suggested that excessive mechanical load influences predominate among these reported non-genetic risk factors [13]. An excessive mechanical stress causes damage to the NP cells, promotes inflammation, breaks the balance between anabolism and catabolism within NP, contributes to extracellular matrix (ECM) degradation [14,15] and finally leads to the degeneration of the NP [16–19].

KRT8 (keratin 8) belongs to the intermediate filament protein family, and plays crucial role in stress protection and mechanical support [20]. As a biomarker of the notochordal cells, from which NP cells were believed to be originated [21–23], the physio-pathological role of KRT8 during disc degeneration has been documented [24]. Our and others' previous study showed a downregulation of KRT8 protein level within human NP tissue as disc degeneration aggravates [25,26]. The KRT8 protein level within NP cells subjected to in vitro compression model also showed a downregulated tendency [27]. These previous results imply a significance and a putative protection role of KRT8 during disc degeneration. However, whether the presence of KRT8 could protect the excessive mechanical load-induced disc degeneration and the underlying mechanism of it remains to be investigated.

Macroautophagy (hereafter autophagy) serves as an evolutionarily conserved catabolic and quality control pathway across all eukaryotes [28,29]. The formation of the phagophore marks the initiation of autophagy. Then, the autophagosome fuses with a lysosome followed by degradation of the contents [30]. As a complicated membrane fusion events, the initiation of the autophagy requires fine orchestration of a number of signaling and membrane trafficking. Appropriate maintenance of autophagy flux is crucial for the survival of NP cells under harsh microenvironment [31,32]. Inhibition of autophagy results in apoptosis of NP cells and disc degeneration [33,34]. Previous studies implied a potential regulatory relationship between KRT8 and autophagy during chemoresistance and oxidative stress resistant [35–37], and a crucial role of autophagy plays during excessive load protection within NP cells has been documented [18,38]. Yet the detailed mechanism by which autophagy was successfully activated and appropriately maintained under overloading remains to be investigated.

Herein, we show that NP specific knockout of *Krt8* in mice aggravates disc degeneration under two load-induced IDD models. Moreover, knockdown of *Krt8* predisposes NP cells to and overexpression of *Krt8* endows NP cells greater resistance to excessive mechanical load-induced apoptosis and degeneration in vitro. Mechanistically, we show that the phosphorylation of KRT8 on Ser43, by mechano stress activated RHOA-PKN (protein kinase N), impedes the trafficking of Golgi resident protein RAB33B, impairs the autophagosome initiation and contributes to disc degeneration. Finally, the therapeutic effects of overexpression of *Krt8* as well as knockdown of *Pkn* were evaluated in a rat tail compression-induced IDD model.

## Results

### Conditional knockout of *Krt8* within NP aggravated load-induced disc degeneration in vivo

To ascertain the role of *Krt8*, which was specifically expressed within NP tissues, during excessive mechanical load-induced disc degeneration, we firstly constructed a *Krt8* NP conditional knockout mice line by Cre-loxP system. The establishment of *Krt8<sup>fl/fl</sup>* mice was demonstrated in the Materials and Methods section (Figure S1A). Male *Krt8<sup>fl/fl</sup>* mice were crossed with female *Lepr-Cre* mice, which was found to be capable of specifically targeting NP cells in our previous study [39], to generate *Lepr-Cre;Krt8<sup>fl/fl</sup>* (hereinafter referred to as cKO) mice (Figure S1B–D). Immunofluorescence (IF) staining of the disc sections confirmed an abolishment of *Krt8* expression within cKO mice in both lumbar (L) as well as coccygeal (Cy) discs (Figure S1E). Up to 4 months postnatal, the cKO mice displayed fairly normal histological structure of the discs, as revealed by hematoxylin-eosin (HE) staining and safranin O-fast green (SOFG) staining (Figure 1A, A', E, E'). The disc height index (DHI), between cKO mice and its' littermate *Krt8<sup>fl/fl</sup>* controls, also showed no statistical significance, as determined by micro-CT scan and X-ray (Figure 1I, I', J, J'). The IVD is embedded within a loaded environment, in which NP cells are exposed to a continuous mechanical load. Since no significant abnormality was observed in cKO mice in regard of disc development, we further challenged the discs of the cKO and control mice by two different mechanical load-induced disc degeneration model, lumbar spine instability model (LSI) for lumbar discs [40], and tail compressive suture model (TCS) for coccygeal discs [41], respectively. 2 months after the LSI surgery, histological, apoptosis, IF and radiological analysis was performed to evaluate the degeneration of the lumbar discs in these four groups (*Krt8<sup>fl/fl</sup>*, cKO, LSI+*Krt8<sup>fl/fl</sup>*; LSI+cKO). The successful establishment of the load-induced disc degeneration by LSI was confirmed by a significant decrease of the ACAN (Aggrecan) level (Figure 1C,G), and a significant increase of the MMP3-positive cells (Figure 1D,H) within the NP, between the *Krt8<sup>fl/fl</sup>* group and the LSI+*Krt8<sup>fl/fl</sup>* group. In addition, a more severe degenerative phenotype was observed between the LSI+*Krt8<sup>fl/fl</sup>* group and the LSI+cKO group, including a significant elevated histological score of the disc, a significant decrease of the ACAN level within in the NP

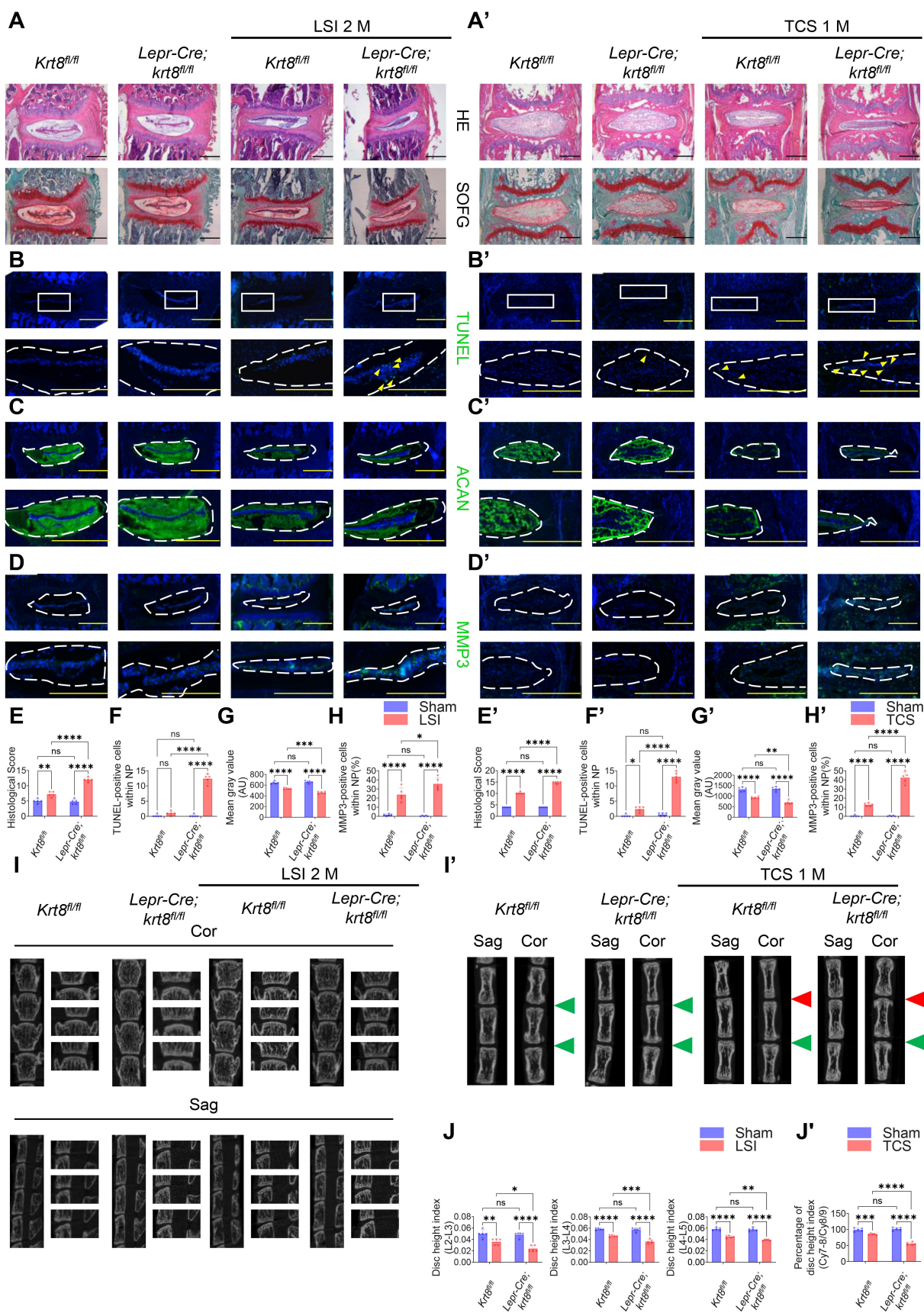


(Figure 1C, G), and a significant increase of the TUNEL-positive cells (Figure 1B, F) as well as MMP3-positive cells (Figure 1D, H) within the NP. The micro-CT analysis also showed a significant decrease of the DHI between the LSI + *Krt8*<sup>fl/fl</sup> group and the LSI+cKO group in all three lumbar segments analyzed (Figure 1I, J).

Similar results were also observed in the TCS model challenged mice. cKO mice displayed a more severe degenerative phenotype after TCS, as determined by histological analysis, IF staining, TUNEL assay, and micro-CT analysis (Figure 1A'-J'). Collectively, these data all showed that conditional knock-out of *Krt8* within NP aggravated load-induced disc degeneration in vivo.

### loss of *Krt8* predisposed NP cells to, and overexpression of *krt8* endowed NP cells with greater resistance to, excessive mechanical load-induced apoptosis and degeneration in vitro

The above results prompted us to investigate whether *Krt8* could rescue the load-induced NP cells' apoptosis and could ameliorate such degenerative phenotype. To this end, we first comprehensively evaluated the expression pattern of *Krt8*, in both mRNA and protein level, during in vivo and in vitro excessive load-induced disc degeneration model. Healthy primary human NP cells and primary rat NP cells were isolated and subjected to an in vitro compression-induced IDD model [17,25,27,42]. The results showed that the transcription of the *Krt8* in both rat and human NP cells was significantly promoted after 12, 24, 36, 48 and 60 h in vitro compression, with the highest transcription level occurred at 36 h (Figure S2A, D), as determined by quantitative reverse-transcriptase polymerase chain reaction (qPCR) analysis. The KRT8 protein level was significantly upregulated after 12, 24 and 36 h, as determined by western blot analysis. However, a significant drop of the KRT8 protein level was noticed in 48 h, compared with 36 h, and such drop tendency continued, to the end of this experiment at 72 h, where the KRT8 protein level was only ~0.5 fold compared with the control group (Figure S2B-F). In addition, the drop of the KRT8 protein was less obvious when co-treated with proteasome inhibitor, MG132 (5  $\mu$ M) (Figure S2G, H); and the increase of the KRT8 protein level between 0-36 h was abolished by the co-treatment of translation inhibitor, cycloheximide (CHX, 20  $\mu$ g/ml) (Figure S2I, J). In summary, all these data indicated that such expression pattern of the *Krt8* within NP cells under in vitro compression was a result of a joint effort from an elevated transcription, translation of the *Krt8* as well as an increased proteasome activity. Similar *Krt8* expression pattern within NP cells could also be observed in an in vivo load-induced IDD model. Sprague-

Dawley (SD) rats were subjected to tail compression-induced IDD model (TCM) [42]. An elevated transcription of the *Krt8* could be observed in 2-W, 4-W and 6-W groups, as determined by qPCR (Figure S2K). The KRT8 protein expression showed a statistically significant increase 4-W groups and a drop in 6-W and 8-W groups, as determined by western blot analysis (Figure S2L, M).

Since an upregulation and a reduction of KRT8 protein level was observed in 24 h and in 48 h, respectively. An siRNA-mediated knockdown of *Krt8* was added to the 24-h group and an adenovirus-mediated overexpression of *Krt8* and *Krt18* was added to the 48-h group, to investigate the role of *Krt8* in load-induced disc degeneration in vitro. Also, since the increased proteasome activity was responsible for the degradation of KRT8 under in vitro compression, MG132 was also introduced to the 48-h group to see if it is possible to rescue the degenerative phenotype by restoring the KRT8 expression through inhibition of the proteasome. The IF of primary rat NP cells (Figure 2A), qPCR (Figure 2B,C) and western blot analysis (Figure 2D, E) all confirmed a successful knockdown and overexpression of *Krt8* in both mRNA and protein level. The results showed that siRNA-mediated knockdown of *Krt8* aggravated degenerative phenotype of the NP cells under in vitro compression for 24 h, as revealed by decreased anabolism level (*Acan*), increased catabolism level (*Mmp3*), increased cytokines production (*Il6*), as determined by qPCR (Figure 2B) and western blot (Figure 2D). Also, a significantly elevated apoptosis of the NP cells was also observed between the 1.0 MPa ( $1 \times 10^6$  pascal, indicating that the pressure within the compression apparatus is  $1 \times 10^6$  pascal) 24-h group and the 1.0 MPa 24-h+si*Krt8* group, as revealed by increased expression of cleaved CASP3 (Figure 2D) and significantly increased apoptotic cells (Figure 2F,H), determined by western blot and flow cytometry, respectively.

In addition, both adenovirus-mediated overexpression of *Krt8* and *Krt18* as well as MG132 treatment successfully rescued the expression of KRT8 protein level after 48 h in vitro compression (Figure 2A, E). However, the rescuing effect could only be observed in the overexpression group, rather than the "MG132" group, as evaluated by anabolism level (*Acan*), catabolism level (*Mmp3*), cytokines production (*Il6*), and apoptotic ratio, as determined by qPCR (Figure 2C), western blot (Figure 2E), and flow cytometry (Figure 2G), respectively. Besides, to rule out the potential protective role by *Krt18* or *Krt19*, both of which could act as a heterodimeric partner of *Krt8*, we also performed extra knockdown of *Krt18* or *Krt19* in 24-h groups, overexpression *Krt8* and *Krt19* [43] or *Krt19* alone, in 48-h groups. The results showed that knockdown of *Krt18* showed a similar result with knockdown

of Fig1c. (G') Fluorescence intensity of ACAN of Fig1c'. (H) Quantification of MMP3-positive cells of Fig1D. (H') Quantification of MMP3-positive cells of Fig1D'. (I) Micro CT analysis of L2-L5 vertebrae. (Cor: coronal plane; Sag: sagittal plane) (I') Micro CT analysis of Cy7-Cy8 vertebrae. (Cor: coronal plane; sag: Sagittal plane) (J) Quantification of DHI of L2-L3, L3-L4, L4-L5 discs. (J') Quantification of percentage of DHI (Cy7-8÷cy8-9).  $n = 5$ ; \*,  $p < 0.05$ ; \*\*,  $p < 0.01$ , \*\*\*,  $p < 0.005$ , \*\*\*\*,  $p < 0.0001$  ns: not statistically significant; Scale bar: 50  $\mu$ m, the yellow triangle indicates TUNEL-positive cells. For all the statistical analyses in this figure, significance was determined by Two-way ANOVA followed by Tukey's multiple comparisons test, and results were shown as mean  $\pm$  S.D.

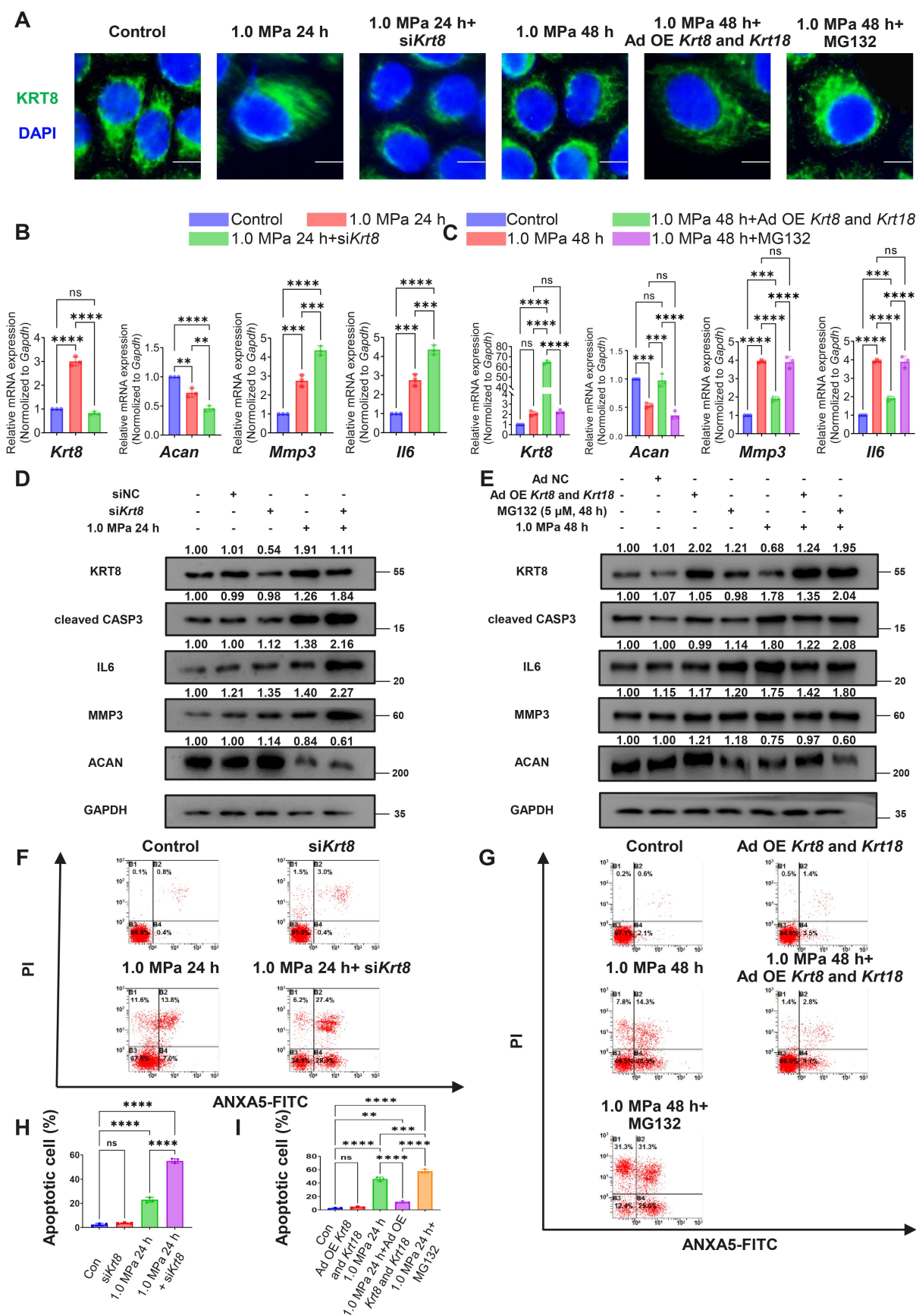


**Figure 2.** Loss of *Krt8* predisposed NP cells to, and overexpression of *Krt8* endowed NP cells with greater resistance to, excessive mechanical load-induced apoptosis and degeneration in vitro. Primary rat NP cells were subjected to in vitro compression model, siRNA-mediated knockdown of *Krt8* or adenovirus-mediated overexpression of *Krt8* and *Krt18* were performed as indicated. **(A)** Representative images of immunofluorescence staining of KRT8 of NP cells. **(B and C)** the transcription of *Krt8*, *Acan*, *Mmp3*, *Il6* from indicated groups, as determined by qPCR. **(D and E)** the protein level of KRT8, cleaved CASP3, IL6, MMP3, ACAN from indicated groups, as determined by western blot. **(F-H)**, and **(I)** Apoptosis of indicated groups evaluated by flowcytometry and its' quantifications. NC: negative control;  $n = 3$ ; \*:  $p < 0.05$ ; \*\*:  $p < 0.01$ , \*\*\*:  $p < 0.005$ , \*\*\*\*:  $p < 0.0001$  ns: not statistically significant; Scale bar: 20  $\mu$ m. For all the statistical analyses in this figure, significance was determined by One-way ANOVA followed by Tukey's multiple comparisons test, and results were shown as mean  $\pm$  S.D.

of *Krt8*, overexpression *Krt8* and *Krt19* showed a similar result with overexpression *Krt8* and *Krt18*. However, knock-down or overexpression of *Krt19* alone showed no significant phenotype changes (Figure S3).

To further validated the detrimental effect of si*Krt8* and unmask the underlying mechanism by which *Krt8* influence the fate and function of NP cells under compression in vitro, mRNA sequencing and bioinformatic analysis was performed (Figure S4A, B). Numbers of differentially expressed genes among groups (Figure S4C) and Kyoto encyclopedia of genes and genomes (KEGG) enrichment of differentially expressed genes among groups (Figure S4D) was reported. Moreover, an activated “proteasome pathway” (KO03050) and an activation of “apoptosis-multiple species pathway” (KO04215) was enriched in “1.0 MPa 24-h” group, as determined by KEGG based gene set enrichment analysis (GSEA) (Figure S4E, F). Also, a detrimental effect of loss of *Krt8* on excessive machinal load-induced NP cells’ degenerative phenotype was also validated by sequencing, including reduced anabolism, elevated catabolism, and increased inflammation cytokines production (Figure S4G).

Collectively, these data illustrated that loss of *Krt8* predisposed NP cells to and overexpression of *Krt8* endowed NP cells greater resistance to excessive mechanical load-induced apoptosis and degeneration in vitro. Noteworthy, only the newly expressed KRT8 protein, rather than the MG132 restored KRT8 protein level, is capable of rescuing the deleterious phenotype under 48-h compression.

#### **A damped autophagosome initiation, caused by impeded trafficking of Golgi resident small GTPase RAB33B, was responsible for the detrimental effect of loss of *Krt8* on NP cells under excessive mechanical load**

Appropriate maintenance of autophagy flux is crucial for the survival of NP cells under harsh microenvironment, e.g., excessive mechanical load [17] or hypoxia [44]. Our [35] and others’ [36,37] previous studies showed a regulatory role of *Krt8* on autophagy. To understand the underlying mechanism by which *Krt8* influence NP cells’ function and survival under excessive mechanical load, we next analysis the autophagy flux in the abovementioned experimental groups. The results showed that the autophagy was activated in the 24-h group, indicated by an elevation of LC3B-positive puncta (Figure 3A, B), an increased conversion of LC3B-II from -I and a degradation of SQSTM1 (Figure 3E). Such activated autophagy was accompanied by a relatively low apoptosis (~75% survival) and a moderate degenerative phenotype, as determined by flow cytometry (Figure 2F) qPCR (Figure 2B) and western blot (Figure 2D). However, a paradoxical LC3B lipidation was observed in the 48-h group, where LC3B-positive puncta (the number of autophagosomes) was significantly decreased, compared with 24-h group (Figure 3C, D, and Figure S4H), yet no significant difference in LC3B-II:I ratio was observed in these two groups, as determined by western blot (Figure 3E, F and Figure S4I), accordingly, the degradation of the SQSTM1 was also blocked (Figure 3E, F and Figure S4J). In addition, such paradoxical results could also be noticed in the 24-h+si*Krt8* group (Figure 3A, B, and E). Moreover, adenovirus-mediated overexpression of *Krt8* and

*Krt18* could rescue the decreased autophagosomes initiation, rebuild the degradation of SQSTM1 and fix the autophagy flux (Figure 3C,D and F). Consistently, MG132-mediated restoration of KRT8 protein level could not mitigate the abovementioned blockage of autophagosomes initiation (Figure 3C,D and F).

Autophagosome formation is a dynamic membrane trafficking event. Previous studies showed that interactions between Atg16L1 and RAB33B [45] were required for LC3B lipidation and autophagosome formation [46]. Knockdown of *Rab33b* reduced the production of LC3B-positive autophagosomes yet no significant difference in LC3B-II: -I ratio was observed [45]. Based on such results, we further checked the expression of *Rab33b* in our experimental groups (*Rab33a* was unable to be detected in rat or human NP cells, Figure S4K, L and M). Results showed a significantly elevated transcription of *Rab33b* in all groups (Figure 3G,H), as determined by qPCR and mRNA sequencing. However, only an increased RAB33B protein level was observed in 24-h and a drop of RAB33B level was observed in 1.0 MPa 24-h +si*Krt8* group and 1.0 MPa 48-h group. Interestingly, overexpression of *Krt8* and *Krt18* could rescue both the drop of RAB33B and a damped autophagosome initiation, yet proteasome inhibitor could only save the RAB33B level (Figure 3J) yet could not rescue the autophagosome initiation (Figure 3C,D).

Trafficking of Golgi-resident small GTPase RAB33B, and the consequent interaction with cytoplasmic ATG16L1 [47], were crucial for autophagosome initiation [29]. Since KRT8 could act as a phosphate “sponge” for stress-activated kinases [48] or could act as a “bridge”, facilitating protein intracellular trafficking [49,50], we then investigate the role of KRT8 during RAB33B trafficking. The whole cell lysate (WCL) protein and the protein from Golgi or endoplasmic reticulum (ER) was extracted and isolated, and RAB33B from WCL was co-immunoprecipitated by KRT8 or ATG16L1 respectively. The results showed an increased binding of RAB33B with KRT8 and ATG16L1 in the 24-h group (Figure 3K), where autophagy flux was appropriately activated. However, a significant and striking elevation of KRT8 bound RAB33B was observed in 1.0 MPa 48-h group, accompanied by a reduction in ATG16L1 bound RAB33B (Figure 3L and Figure S4N, O). Also, a drop of ATG16L1 bound RAB33B was also noticed in 1.0 MPa 24-h+si*Krt8* group. Consistently, only the adenovirus-mediated overexpression of KRT8 protein level, rather than the MG132 rescued KRT8, could rescue the drop of ATG16L1 bound RAB33B (Figure 3). The results from this section clearly demonstrated that KRT8 is essential for the trafficking of RAB33B from Golgi to ATG16L1. Moreover, proteasome inhibitor restored KRT8 protein level was not a “functional” KRT8 anymore and could not facilitate the trafficking of RAB33B.

#### **The phosphorylation of KRT8 on Ser43 impeded the trafficking of RAB33B from Golgi to autophagosome through trapping RAB33B with p-Ser43 KRT8**

The obstructed trafficking of RAB33B under excessive mechanical load, and the rescue of it by the overexpressed KRT8 protein level, showed a regulatory relationship between

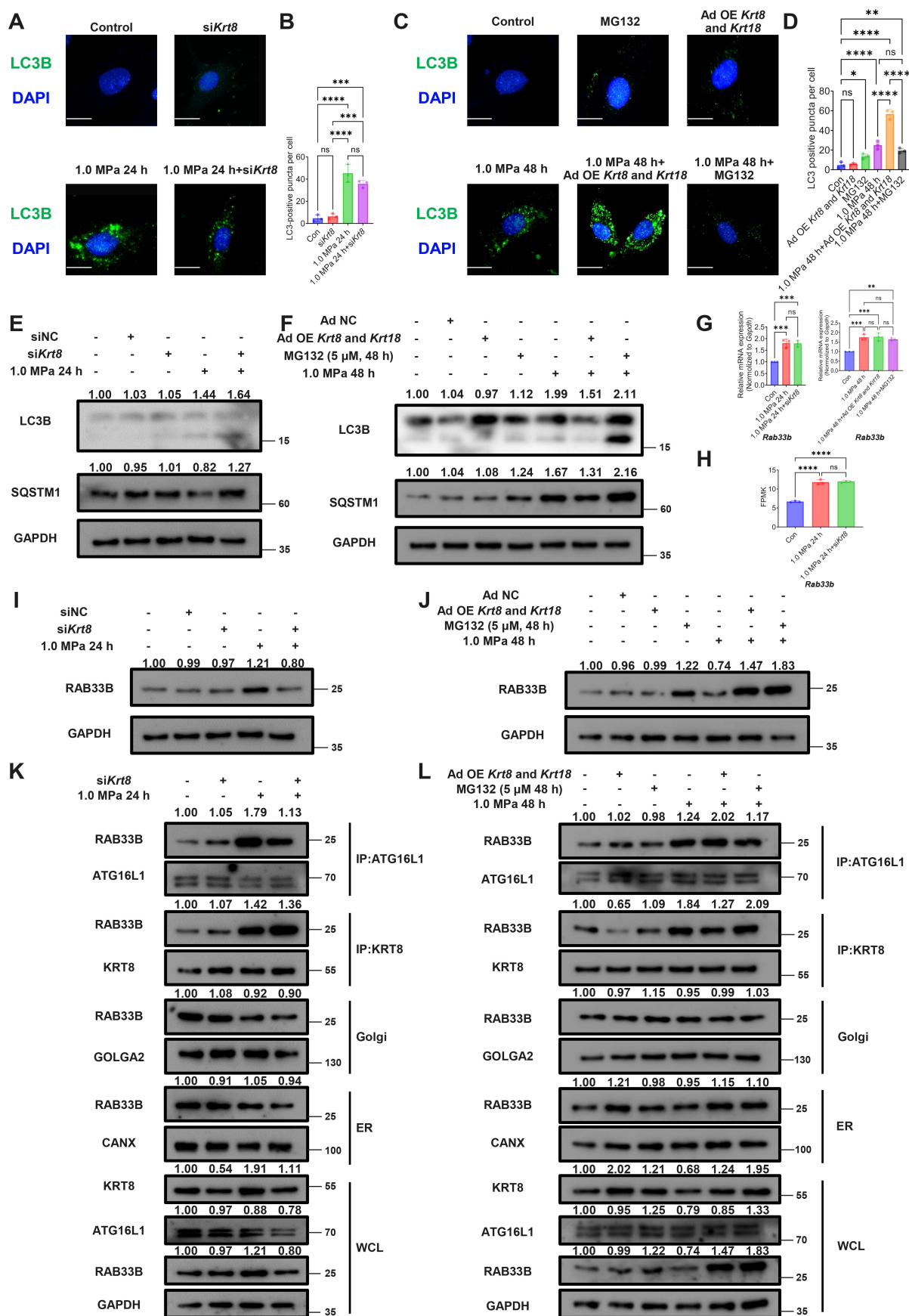


**Figure 3.** A damped autophagosome initiation, caused by impeded trafficking of Golgi resident small GTPase RAB33B, was responsible for the detrimental effect of loss of *Krt8* on NP cells under excessive mechanical load. Primary rat NP cells were subjected to in vitro compression model, *siKrt8* or overexpression of *Krt8* and *Krt18* were performed as indicated. (A–D) Representative images of immunofluorescence staining of LC3B of NP cells and their quantifications. (E and F) the protein level of LC3B, SQSTM1 from indicated groups. (G) The transcription of *Rab33b* form indicated groups, as determined by qPCR. (H) the transcription of *Rab33b* form indicated

the presence of KRT8 and the trafficking of RAB33B. However, the paradoxical results that only the newly expressed KRT8, rather than MG132 restored KRT8 protein expression, could rescue the trafficking of RAB33B, warranted the investigation of an underlying mechanism, rather than the whole protein level of KRT8, for example, mechanisms involving the post translational modifications of KRT8.

Keratins are functionally regulated by post translational modifications (PTMs) [51], and phosphorylation of keratins has been known to modulate their interactions with other proteins [52]. Our previous study confirmed a phosphorylation of KRT8 within NP cells under excessive mechanical load in vitro [27]. Results from current study showed a strong positive correlation between p-KRT8 and KRT8 bound RAB33B, accompanied by a corresponding reduction of ATG16L1 bound RAB33B (Figure 4A). To further elucidate the role of KRT8 phosphorylation during excessive mechanical load-induced disc degeneration, we employed quantitative phosphoproteomic analysis to evaluate the phosphorylation status of KRT8 comprehensively and accurately, under in vivo compression-induced rat tail disc degeneration model (Figure S5A). Total 27 phosphorylated sites of KRT8 were identified (Figure S5C), and the top 6 sites (>1.75 fold change, Ser27, 35, 36, 43, 51, Thr305) were included for further study. Mutations of each included phosphorylated sites to aspartic acid (D) were constructed respectively, and adenovirus-mediated overexpression of each mutated KRT8 protein were performed, to evaluate the rescuing effects after 48 h in vitro compression. The results showed that all 6 mutations could be stabilized expressed, which indicated that mutations of these sites to D did not impede their binding with KRT18 (Figure 4B). Moreover, 5 mutations among these tested mutations showed a comparable rescuing effect with wild-type KRT8, except for S43D, whose overexpression did not facilitate the trafficking of RAB33B and showed no significant rescuing effect, as indicated by a higher KRT8 bound RAB33B, a lower ATG16L1 bound RAB33B (Figure 4B), and a significantly higher apoptosis (Figure S5D, E), after 48 h in vitro compression. These results clearly demonstrated that KRT8 plays crucial role in maintaining autophagy flux within NP cells under excessive mechanical load, and phosphorylation of KRT8 on Ser43 blocked the autophagosome initiation by impeding the trafficking of RAB33B from Golgi to autophagosome through trapping RAB33B with p-Ser43 KRT8.

In addition, serine residue 43 (Ser43) of rat KRT8 protein and the surrounding sequence was highly conserved in other species (Figure S5F), which further warrants the investigation of a detailed mechanism, by which Ser43 of KRT8 was phosphorylated under excessive mechanical load. To this end, a polyclonal phosphorylation site – specific antibody targeting

rat p-Ser43 KRT8 was generated, based on peptide “FSRVG-(p-S)-SSS” (Figure S5G, H).

### **Mechano stress-induced activation of RHOA-PKN was responsible for the phosphorylation of KRT8 on Ser43 under excessive mechanical load**

In an attempt to identify the protein kinases responsible for the phosphorylation of Ser43 of KRT8 under excessive mechanical load, Group-based Prediction System (GPS) V5.0 software was employed to predict the protein kinase based on the motifs surrounding the phosphorylated Ser43 of rat KRT8 [53]. Top 5 predicted kinases based on the prediction score was included for further study (Figure S5I and J, *Tbk1* and *Pkn3* was not expressed in primary rat NP cells as mRNA sequencing data shows). siRNA-mediated knockdown of *Plk4*, *Tbk1*, *Pkn1*, *Pkn2*, *Pkn1* and *Pkn2*, *Srpk1*, and *Ttbk1* was added to the 48-h compression group, and the results showed that both *Pkn1* and *Pkn2* knockdown, could reduce the protein level of p-Ser43 KRT8, facilitate the trafficking of RAB33B, indicated by the reduced KRT8 bound RAB33B and promoted ATG16L1 bound RAB33B (Figure 4C), and could rescue the apoptosis the NP cells (Figure 4D and Figure S6A). Noteworthy, a combination of si*Pkn1* and si*Pkn2* showed a robust reduction of phosphorylation of Ser43 of KRT8 (Figure 4C), significantly improved the survival of NP cells under 48 h in vitro compression, compared with si*Pkn1* or si*Pkn2* alone (Figure 4D and Figure S6A). In addition, siRNA-mediated knockdown of *Pkn1* and *Pkn2* could partially rescue the degenerative phenotype of NP cells under 48 h in vitro compression (Figure 4E). Moreover, PKN1 and PKN2 were activated under both in vivo and in vitro compression within NP cells. The quantitative phosphoproteomic analysis of NP tissue from rat tail compression-induced IDD model showed a 1.5-fold elevation of p-Thr778 PKN1 and a 1.7-fold elevation of p-Thr702 PKN2 (Figure S5K). Also, western blot analysis also confirmed an activation of PKN1 and PKN2 within NP cells in vitro compression model, in a time and pressure dependent manner (Figure 4F,G). Next, we investigated the mechanism by which PKN1 and PKN2 were activated. PKNs are serine/threonine kinases that have been shown to be activated by mechanical sensitive RHOA pathway [54]. Also, our previous study also confirmed an activation of RHOA pathway within NP cells under in vitro compression-induced IDD model [42]. In addition, Reactome based GSEA also showed an enrichment of “R-RNO-5625740: RHO GTPases activate PKNs”, which indicated an activation of PKNs by RHO-GTPases in primary rat NP cells, after 1.0 MPa, 24 h in vitro compression (Figure 4H). To verify such results, RhoA inhibitor C3 transferase (50 nmol/l) was added to the in vitro compression groups. The

groups, as determined by mRNA sequencing. (I and J) the protein level of RAB33B from indicated groups, as determined by western blot. (K and L) ATG16L1 bound RAB33B, KRT8 bound RAB33B, Golgi localized RAB33B, ER localized RAB33B and RAB33B from whole cell lysate (WCL) from indicated groups, as determined by western blot. NC: negative control; n = 3; \*: p<0.05; \*\*: p<0.01, \*\*\*: p<0.005, \*\*\*\*: p<0.0001 ns: not statistically significant; Scale bar: 20 μm. For all the statistical analyses in this figure, significance was determined by One-way ANOVA followed by Tukey's multiple comparisons test, and results were shown as mean ± S.D.



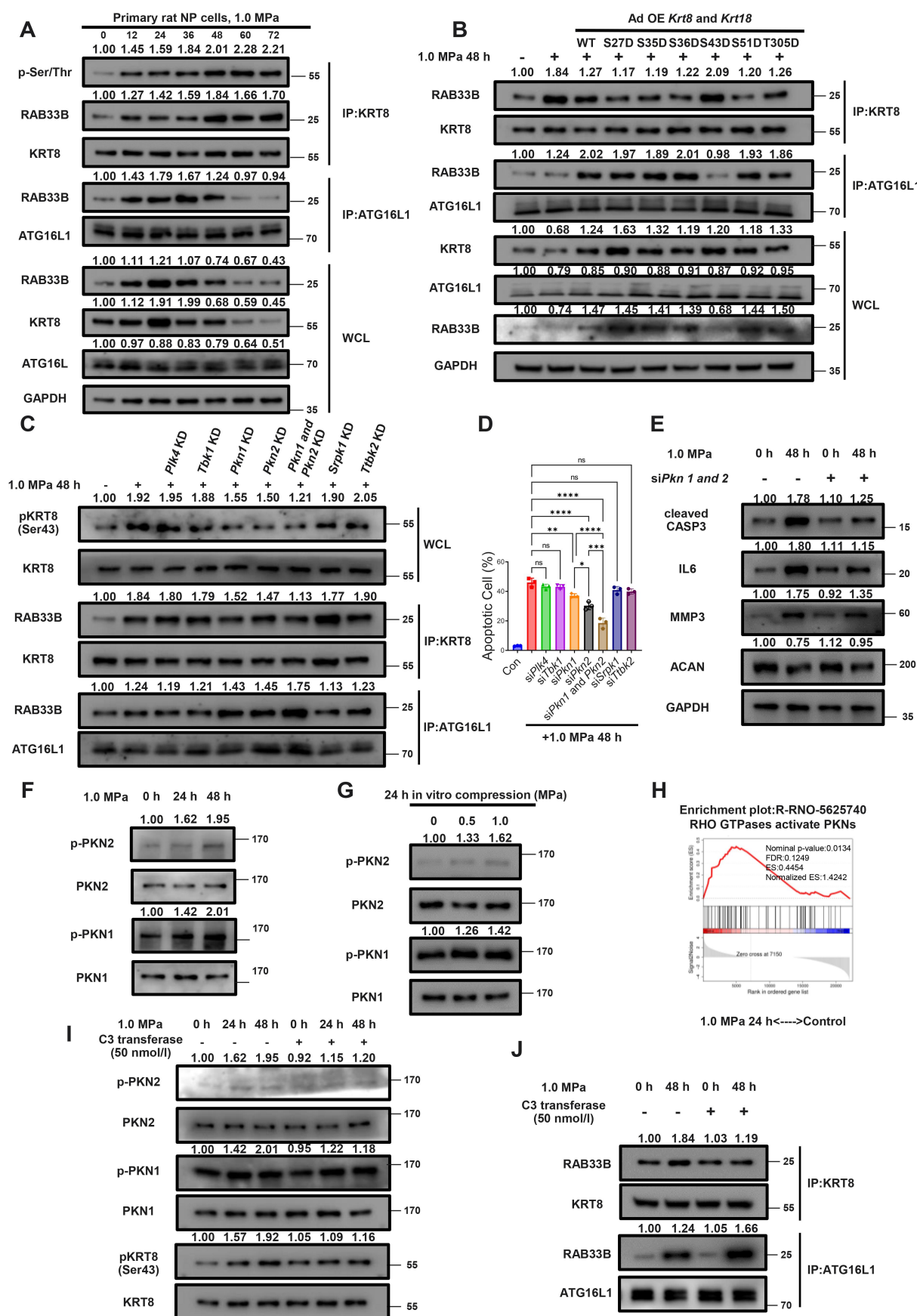


**Figure 4.** The phosphorylation of KRT8 on Ser43 impeded the trafficking of RAB33B from Golgi to autophagosome through trapping RAB33B with p-Ser43 KRT8, and mechano stress-induced activation of RHOA-PKN was responsible for the phosphorylation of KRT8 on Ser43 under excessive mechanical load. Primary rat NP cells were subjected to in vitro compression for indicated time. (A) the phosphorylation of KRT8, KRT8 bound RAB33B, ATG16L1 bound RBA33B, and KRT8, RAB33B, ATG16L1 protein from WCL of indicated groups were determined by western blot. Primary rat NP cells were subjected to in vitro compression for 48 h, accompanied

results showed that RHOA inhibition strikingly reduced the activation of PKN1 and PKN2, as indicated by decreased p-PKN1 and p-PKN2 by western blot analysis (Figure 4I). Also, the phosphorylation of KRT8 on Ser43 was also suppressed (Figure 4I), and the trafficking of RAB33B was rescued by RHOA inhibition (Figure 4J). Together, these data clearly showed that excessive mechanical stress-induced activation of RHOA-PKN was responsible for the phosphorylation of KRT8 on Ser43 under excessive mechanical load, siRNA-mediated ablation of *Pkn1* and *Pkn2* or pharmaceutical inhibition of RHOA could abolish the phosphorylation of KRT8 on Ser43 under excessive mechanical load, and could rescue the apoptosis and the degenerative phenotype of NP cells under in vitro compression.

#### **AAV5-mediated overexpression of *Krt8* as well as shRNA-mediated knockdown of *Pkn1* and *Pkn2*, at early stage of TCM, ameliorated rat tail disc degeneration**

Results from in vitro experiments indicated a potential therapeutic effect of overexpression of *Krt8* or knockdown of *Pkn1* and *Pkn2* in ameliorating degenerative phenotype and in rescuing apoptosis of NP cells under excessive mechanical load. We then evaluated the therapeutic effects of these approaches in rat tail compression-induced IDD model (TCM) in vivo. 8-week-old male SD rats were randomly divided into 4 groups: control group, TCM+AAV-Scrambled group, TCM+AAV-OE-*Krt8* and *Krt18* (OE) group, TCM+AAV-sh-*Pkn1* and *Pkn2* (KD) group. In this experiment, AAV was injected into the NP of the Cy7-Cy8 IVD, immediately after the TCM surgery, to evaluate therapeutic effect of the overexpression of *Krt8* or inhibition of *Pkn1* and *Pkn2* at early stage of the IDD (Figure 5A,B). 8 weeks after the procedure, western blot analysis showed that overexpression of *Krt8* and *Krt18*, as well as knockdown of *Pkn1* and *Pkn2*, reduced the protein level of cleaved CASP3 (Figure 5C). Also, promoted anabolism level (ACAN), reduced catabolism level (MMP3) and cytokines production (IL6) was also observed in OE and KD group (Figure 5C). Meanwhile, the HE and SOFG staining showed an ameliorated degenerative phenotype of NP tissue, as reaved by a reduced histological score in these two groups (Figure 5D,E). In addition, the MRI analysis showed a reduced Pfirrmann grade (Figure 5F,G), and the X-ray also confirmed a significantly elevation of percentage of disc height index (Cy7–8 and Cy8–9) in these

rescued groups (Figure 5H,I). Collectively, these data validated the rescuing effect of both overexpression of *Krt8* as well as knockdown of *Pkn1* and *Pkn2*, when treated at early stage of TCM, ameliorated disc degeneration in vivo.

#### **The therapeutical effect of shRNA-mediated knockdown of *Pkn1* and *Pkn2* or AAV5-mediated of *Krt8* and *Krt18* at late stage of compression-induced disc degeneration model**

Since the abovementioned data showed that it was not until 6 weeks after TCM, did the KRT8 protein level within NP tissue showed a significant reduction. We then evaluated the therapeutical effect of knockdown of *Pkn1* and *Pkn2* or overexpression of *Krt8* treated at late stage of TCM. In this experiment, AAV or shRNA was injected into the NP of the Cy7-Cy8 IVD, 6 weeks after the TCM surgery (Figure 6A,B). 14 weeks after the TCM surgery (8 weeks after the injection), all the experimental subjects were sacrificed. The western blot analysis showed that AAV-mediated overexpression of *Krt8* and *Krt18* failed to significantly promote the KRT8 protein level within the NP cells (Figure 6C) and could not ameliorated load-induced disc degeneration. However, knockdown of *Pkn1* and *Pkn2* reduced the protein level of cleaved CASP3 within NP cells (Figure 6C). Improved anabolism level (ACAN) reduced catabolism level (MMP3) and cytokines production (IL6) could also be observed in KD group (Figure 6C). In addition, the reduced histology score indicated an ameliorated degenerative phenotype of IDD in KD group (Figure 6D,E), the MRI analysis also showed a reduced Pfirrmann grade (Figure 6F,G), and the X-ray confirmed a significantly elevation of percentage of disc height index (Cy7–8 and Cy8–9) in KD group (Figure 6H,I). However, no therapeutic effect was observed in OE group, as evaluated by western blot analysis (Figure 6C), histology analysis (Figure 6D,E), MRI (Figure 6F,G) or X-ray scan (Figure 6H,I). Collectively, these data indicated that only knockdown of *Pkn1* and *Pkn2*, when treated at late stage of TCM, ameliorated disc degeneration in vivo.

## **Discussion**

Epidemiology study reported that people more often leave their job because of LBP than diabetes, hypertension, neoplasm, asthma, heart and respiratory disease combined [55]. The high economic as well as medical burden of the degenerative disc related diseases warrants the investigation of the pathogenesis and effective non-surgical treatment approaches to the IDD [1]. Excessive mechanical load (or overloading) is a well-documented independent

by overexpression of wild-type *Krt8* or mutant *Krt8* as indicated. (B) KRT8 bound RAB33B, ATG16L1 bound RBA33B, and KRT8, RAB33B, ATG16L1 protein from WCL of indicated groups were determined by western blot. Primary rat NP cells were subjected to in vitro compression for 48 h, accompanied by siRNA-mediated knockdown of predicted protein kinases. (C) the phosphorylation of KRT8, KRT8 bound RAB33B and ATG16L1 bound RBA33B, of indicated groups were determined by western blot. (D) the quantification of apoptotic cells from indicated groups, determined by flowcytometry. Primary rat NP cells were subjected to in vitro compression for 48 h, accompanied by siRNA-mediated knockdown of *Pkn1* and *Pkn2* or not. (E) the protein level of cleaved CASP3, IL6, MMP3 and ACAN from indicated groups, as determined by western blot. Primary rat NP cells were subjected to in vitro compression for indicated time period or pressure. (F and G) the activation of PKN1 and PKN2, revealed by the phosphorylation of PKN1 and PKN2, was determine by western blot. (H) GSEA analysis showed an activation of R-RNO-5625740 after 1.0 MPa 24 h compression. Primary rat NP cells were subjected to in vitro compression for indicated period of time, accompanied by treatment of RHOA inhibitor C3 transferase (50 nmol/l) or not. (I) the activation of PKN1 and PKN2, revealed by the phosphorylation of PKN1 and PKN2, and the phosphorylation of KRT8 on Ser43, was determine by western blot. (J) KRT8 bound RAB33B and ATG16L1 bound RAB33B were determined by western blot. n = 3; \*: p<0.05; \*\*: p<0.01, \*\*\*: p<0.005, \*\*\*\*: p<0.0001 ns: not statistically significant. For all the statistical analyses in this figure, significance was determined by One-way ANOVA followed by Tukey's multiple comparisons test, and results were shown as mean ± S.D.

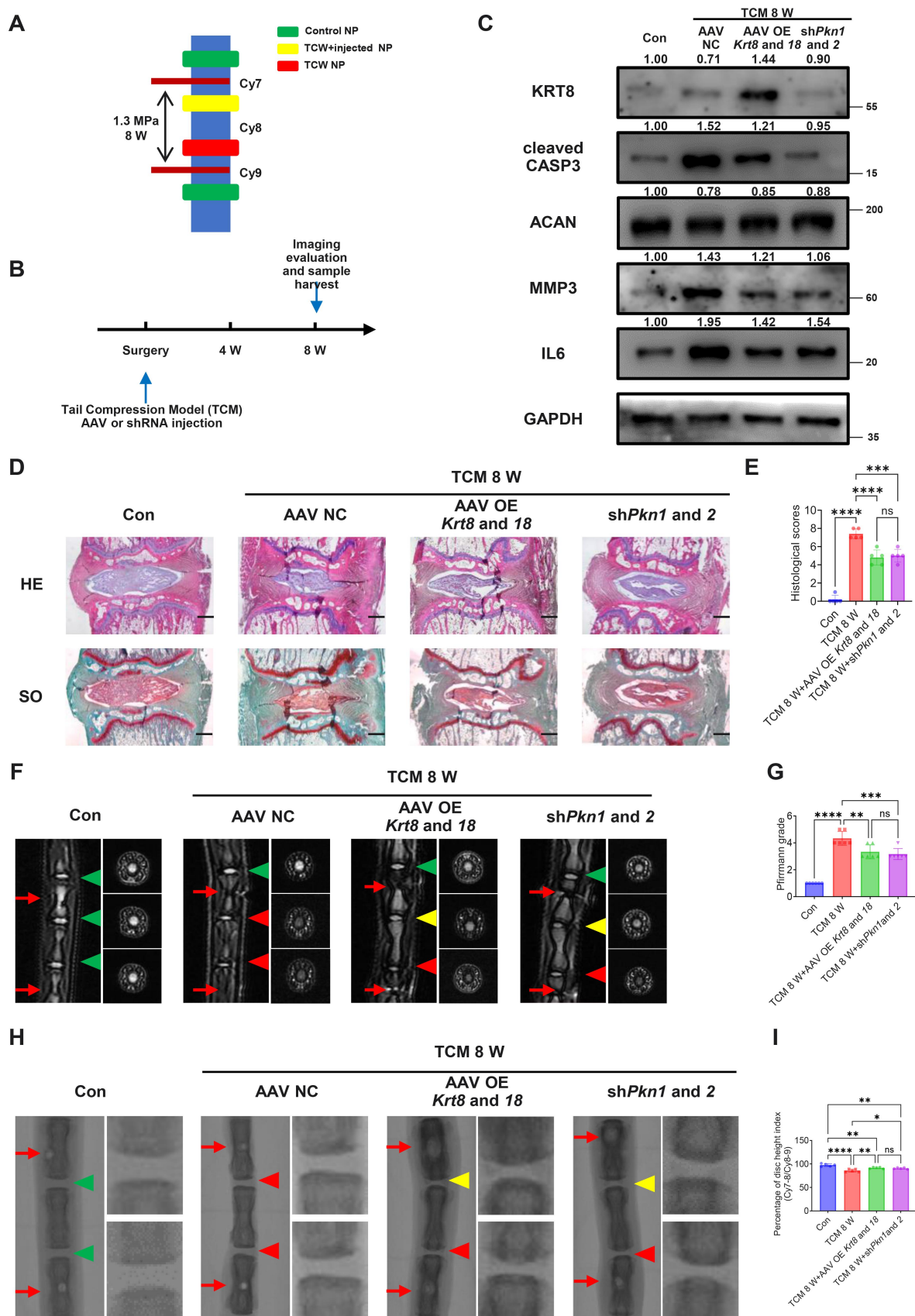


**Figure 5.** AAV5-mediated overexpression of *Krt8* as well as shRNA-mediated knockdown of *Pkn1* and *Pkn2*, at early stage of TCM, ameliorated rat tail disc degeneration. Eight-week-old male SD rats were subjected to TCM. In this experiment, AAV or shRNA was injected into the NP of the Cy7-Cy8 IVD, immediately after the TCM surgery. **(A and B)** Summary of the design of the current study. **(C)** the protein level of KRT8, cleaved CASP3, ACAN, MMP3, and IL6 from indicated groups were determined by western blot. **(D and E)** HE, SOFG staining and histological score of Cy7-Cy8 disc sections. **(F and G)** MRI analysis, Pfirrmann grading and its'

pathogenetic factor of the IDD [56,57]. The elucidation of the detailed mechanism of overloading-induced disc degeneration would be of great help to the development of new therapeutic approaches to the IDD and could provide more insights into the pathogenesis of other load-induced pathologies, heart failure for example.

Keratins have a cell-specific expression pattern among different epithelial originated cell types, where they execute protective actions when reacted to mechanical and non-mechanical stress. Our previous study showed that upregulation of the *Krt8* is closely linked to the chemoresistance of the chordoma cells, knockdown of *Krt8* chemosensitizes the chordoma cells through aggravating unfolded protein response and blocking autophagy [35]. Also, the cytoprotective role of *Krt8* could also be seen in retinal pigment epithelium cells, where KRT8 could protect apoptotic death from reactive oxygen species (ROS). In addition, the function of keratins is largely dependent on the post translational modification (PTM) statuses [52]. A general role of keratin phosphorylation, which is modulated by kinases and phosphatases, is to facilitate keratin reorganization, which considered to be a universal response to stress, by targeting Ser/Thr residues, typically in the head or tail domains of the keratins [58]. Moreover, a “sponge” like function of KRT8 has been proposed where KRT8 could “absorb” the phosphorylation from stress-activated kinases [48]. In NP cells, *Krt8*, *18* and *19* are co-expressed. Our results showed that *Krt8*, rather than *Krt18* or *Krt19*, plays a crucial role in the development of overloading-induced IDD. NP conditional knockout of *Krt8* (*Lepr-Cre;Krt8<sup>fl/fl</sup>*) aggravated load-induced disc degeneration in vivo, siRNA-mediated knockdown of *Krt8* predisposed NP cells to and adenovirus-mediated overexpression of *Krt8* endowed NP cells greater resistance to excessive mechanical load-induced apoptosis and degeneration in vitro. Mechanistically, loss of *Krt8* damped autophagosome initiation, by impeding the trafficking of Golgi resident small GTPase RAB33B.

Interestingly, the results, that only newly expressed KRT8 protein, rather than MG132-induced restoration of KRT8 protein level could save the apoptosis and mitigate the degenerative phenotype, further warranted the investigation of an underlying mechanism involving the PTM of keratins. Since our previous study, as well as the current report, all showed an upregulation of phosphorylation of KRT8 within NP cells under compression in vitro, quantitative phosphoproteomic analysis was employed to evaluate the phosphorylation status of KRT8 under in vivo compression-induced IDD model. Also, in vitro amino acid-mutant experiments showed that overexpression of S43D mutated KRT8 could not save the apoptosis and degenerative phenotype under excessive mechanical load. Next, GPS algorithm based bioinformatic prediction and in vitro siRNA-mediated loss of function experiments confirmed that PKN1 and PKN2 was responsible for the phosphorylation of KRT8 on Ser43, and the activation of PKN1 and PKN2 was also validated by quantitative phosphoproteomic analysis, GESA,

and in vitro western blot analysis. PKN1 and PKN2 belong to the protein kinase C superfamily, sharing a characteristic C-terminal catalytic domain, and the N-terminal domain confers binding and regulation by RHOA, RHOB or RHOC, fatty acids, and phospholipids [59]. The mechanical stress activated RHOA-PKNs has been documented in the hypertension-induced heart failure, and ablation of *Pkn1* and *Pkn2* partially rescued the heart function subjected to heart failure animal model [60]. In addition, the mechanical-induced activation of RhoA within NP cells was also observed in our previous research [42]. Indeed, in vitro inhibition of RHOA suppressed the activation of PKN1 and PKN2, reduced the protein level of p-Ser43 KRT8, saved the trafficking of RAB33B, and mitigated the degenerative phenotype of NP cells under in vitro compression.

Results from the in vivo experiments, evaluating the rescuing effect of overexpression of *Krt8* and knockdown of *Pkn*, were also of great interests. The results showed that AAV-mediated overexpression of *Krt8* as well as shRNA-mediated knockdown of *Pkn* all ameliorated the load-induced disc degeneration, in experiments where surgery was immediately followed by injection of AAV or shRNA. However, if the injection was performed 6 weeks after the TCM surgery, only knockdown of *Pkn1* and *Pkn2* could partially save the disc degeneration, yet overexpression of *Krt8* failed to overexpress the KRT8 protein and could not rescue the load-induced IDD ( $n = 5$  in the reported data, total 15 animals was injected by 3 experienced technicians in 3 independent series of experiments, to rule out the possible operational mistakes). The possibility of malfunction of the AAV vector was also ruled out since another AAV-mediated shRNA successfully knocked down target gene in another experimental group (data not shown), and AAV from same batch successfully overexpressed the KRT8 protein level when injected immediately after the TCM surgery. One possible explanation to such results is that 6 weeks after the TCM surgery, the living cells within the NP tissue was not adequate or viable enough to synthesize exogenous protein. The intervertebral disc is a complex yet biologically aviate biomechanical system. As the largest avascular tissue of the human body, passive diffusion through the CEP result in not only poor nutrition but also low oxygen tension at the center of the NP [61]. The calcification of the CEP, under load-induced IDD, would further deteriorate the harsh environment of the NP [57,62]. Under such circumstance, a compromised efficient of AAV-mediated overexpression of genes is predictable. On the contrary, shRNA-mediated knockdown of certain genes is still working since the delivery or functioning of the shRNA only consume little energy of the resident cells within the NP.

As the largest avascular organ in the body, the central NP was embedded within a low nutrition supply, high lactic acid microenvironment [63]. The activation and utilization of

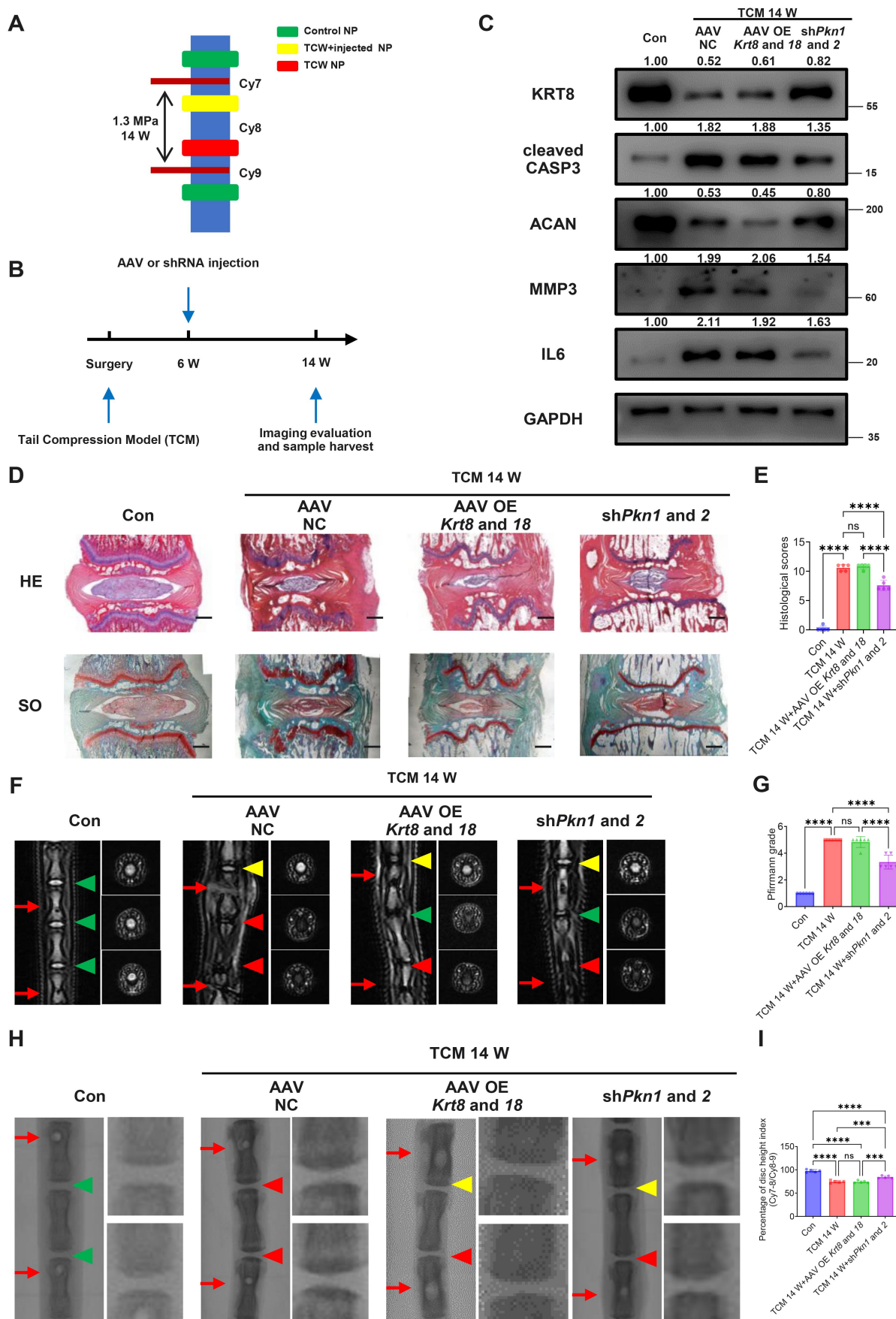


**Figure 6.** The therapeutic effect of AAV-mediated knockdown of *Pkn1* and *Pkn2* or overexpression of *Krt8* and *Krt18* at late stage of compression-induced disc degeneration model. 8-week-old male SD rats were subjected to TCM. In this experiment, AAV or shRNA was injected into the NP of the Cy7-Cy8 IVD, 6 weeks after the TCM surgery. **(A and B)** Summary of the design of the current study. **(C)** the protein level of KRT8, cleaved CASP3, ACAN, MMP3, and IL6 from indicated groups

autophagy became more important for NP cells' survival under such harsh conditions. Serial studies conducted by Yurube et al validated an indispensable role of autophagy during disc homeostasis maintenance [18,31–34,38], loss of *Atg5*-mediated and mTOR signaling pathway dependent autophagy predisposed NP cells to senescence and apoptosis. Moreover, the necessary involvement of autophagy within NP cells could be also seen under hypoxia [17,44], excessive mechanical loading [14,15,19], and inflammatory factors stimulation [64]. Consistent with previous reports, our manuscript showed an activation of autophagy under in vitro compression, and such activation of autophagy was clearly dependent on the presence of cytoskeletal protein KRT8. Furthermore, discovery driven experiments revealed that phosphorylation of KRT8 by PKN1 and PKN2 on Ser43 impaired autophagosome initiation by retaining the RABB3B and therefore blocking the interaction of RABB3BABB 3B and ATG16L1.

The significance of excessive mechanical stress in the development of a number of diseases has been rapidly acknowledged, recently [18,33,65]. A number of studies showed that overloading (or increased mechanical pressure) and inflammation are synonymous [19,66]. Overloading-induced fibrosis and inflammation of healthy tissue could in turn generate or transduce more mechanical stress into the tissue, forming a vicious circle [14,15,67]. In our study, we showed that targeting mechano-stress activated PKNs rebuilt autophagy flux, greatly reduced the production of inflammation cytokine production, rebalanced the anabolism and catabolism within NP cells, and contributed to the homeostasis maintenance of extracellular matrix. The current study supports that therapeutic approaches targeting mechano transduction pathways or “mechano-therapeutics” represent novel and effective treatment strategies to musculoskeletal degenerative disease, cancers [68], or neurodegenerative diseases [69].

Notably, limitations of the current study exist, and results of the works need to be interpreted with caution. To begin with, the NP cells are constantly exposed to hypoxia microenvironment under physiological conditions, the standard cell culture condition exploited in the current study may not fully represents the living condition of the in vivo NP. Secondly, 8 weeks and 14 weeks of sustained rat tail compression are relatively long period time of compression and may lead to irreversible pathological development of the IDD and could not perfectly reflect all aspects of human disc degeneration. Thirdly, murine animals contain notochordal like NP cells throughout life, yet these cells disappeared at early stage of human life. The differences between the developmental biology of murine and human needs to be addressed when interpreting the results of the current work.

To conclude, our study validated a protective role of *Krt8* during overloading-induced IDD and demonstrated that targeting overloading activated of PKNs could be a novel and effective approach to mechano stress-induced pathologies with a wider window of therapeutic opportunity (Figure 7).

## Materials and methods

### Patient samples

Human NP samples were obtained from 12 patients (6 male and 6 females, mean age = 23.08 ± 2.19 years old) who received surgery for scoliosis. The modified Pfirrmann grading system by MRI scan was employed to evaluate the degree of disc degeneration [70]. The Grade I and II discs were defined as “healthy NP tissue” and was collected for primary NP cells isolation. NP tissue was taken from the inner part of IVD, which was gelatinous. Different disc regions were cleanly separated from each other and clearly distinguished for unambiguous dissection. Ethics approval was obtained from the Institutional Review Board of Xijing Hospital of the Fourth Military Medical University, and informed consent was obtained from each donor.

### Animals

All animal experiments were approved by the Institutional Animal Care and Use Committee of the Fourth Military Medical University. The care and protection of experimental animals were in accordance with the guidelines and regulations of animals of the US National Institutes of Health and the Chinese National Institute of Health. Animals were housed under controlled temperature of 24 ± 1°C with a 12-h light/dark cycle. The wildtype C57BL/6J mice and Sprague Dawley (SD) rats were obtained from the Animal Center of the Fourth Military Medical University. The *Lepr-Cre* mice (007909) was purchased from the Jackson Laboratory (USA) [39]. The *Krt8<sup>fl/fl</sup>* mice were generated in the C57BL/6 background (summarized in Figure S1A). Briefly, the *Krt8* gene is located on mouse chromosome 15. Nine exons have been identified. The exon 2 was selected as a conditional knockout region, whose deletion could result in the loss of function of the mouse *Krt8* gene. In the targeting vector, the “SA-2A-dTomato-PolyA” cassette was cloned downstream of exon 2 in the reverse orientation. The cKO region and the reverse “SA-2A-dTomato-PolyA” cassette will be flanked with loxP and lox2272 sites. The constitutive KO allele will be obtained after Cre-mediated recombination. The *Krt8<sup>fl/fl</sup>* mice was obtained by intercrossing of *krt8<sup>fl/+</sup>* mice. Both *Krt8<sup>fl/+</sup>* and *Krt8<sup>fl/fl</sup>* mice were viable and fertile and exhibited no apparent phenotypic changes or modification of behavior. The

---

were determined by western blot. (D and E) HE, SOFG staining and histological score of Cy7-Cy8 disc sections. (F and G) MRI analysis, Pfirrmann grading and its' quantification of coccygeal discs. (H and I) X-ray analysis, and quantification of percentage of DHI (Cy7–8/Cy8/9) of coccygeal discs.  $n = 5$ ; \*:  $p < 0.05$ ; \*\*:  $p < 0.01$ , \*\*\*:  $p < 0.005$ , \*\*\*\*:  $p < 0.0001$  ns: not statistically significant; Scale bar: 500  $\mu\text{m}$ , the red arrow indicates compression apparatus puncture points; the green triangle indicates control discs; the red triangle indicates degenerated discs; and the yellow triangle indicates AAV or shRNA injected discs. For all the statistical analyses in this figure, significance was determined by One-way ANOVA followed by Tukey's multiple comparisons test, and results were shown as mean ± S.D.

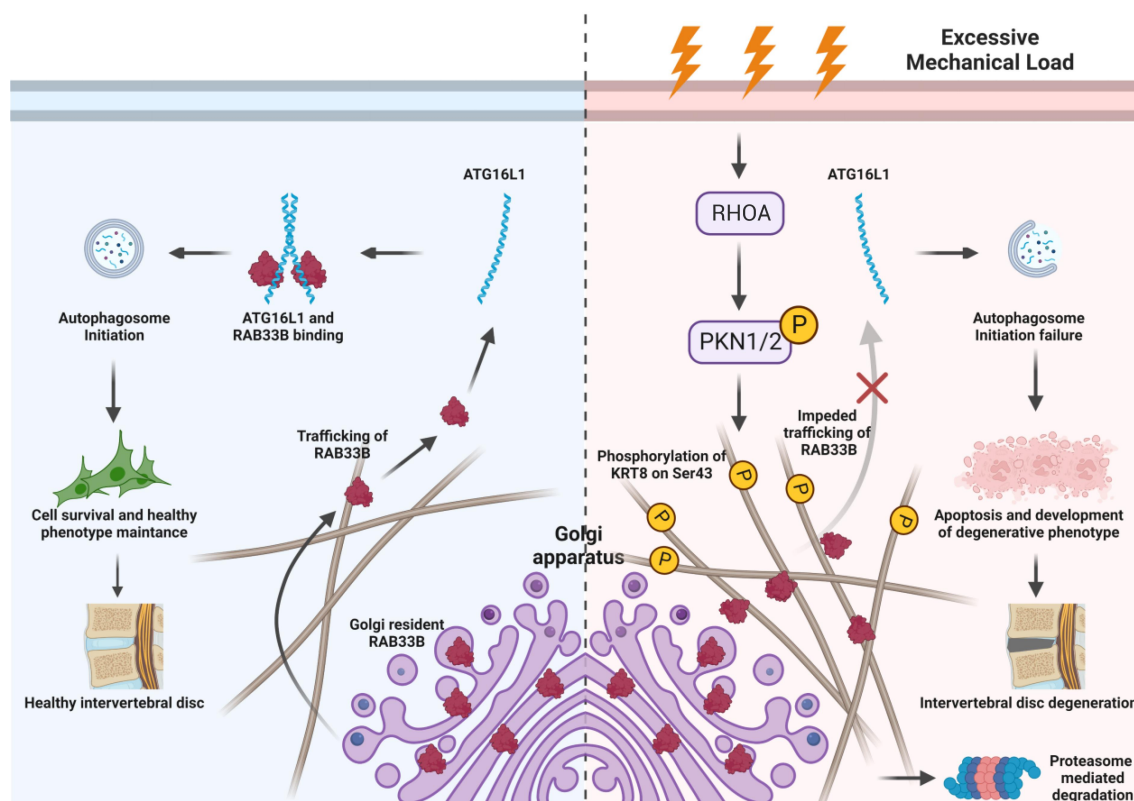


**Figure 7.** Schematic diagram of the current study. Phosphorylation of Ser43 on KRT8 by excessive mechanical load activated RHOA-PKN impedes the trafficking of Golgi resident protein RAB33B, by trapping RAB33B with *p*-Ser43 KRT8, impairs autophagosome initiation and contributes to disc degeneration.

genotyping strategy of *Krt8<sup>fl/fl</sup>* mice was summarized in Fig. S1A and C, and the genotyping results were illustrated in Figure S1D.

### Primary NP cells isolation, culture, and in vitro compression model

A total of 32 male Sprague-Dawley (SD) rats (8-weeks old, skeletally mature) were used for the isolation of primary rat NP cells in this study. Rats were euthanized by inhaling an excessive amount of isoflurane. Rat tails were removed under aseptic conditions, and coccygeal IVDs were separated. The gelatinous NP tissue was separated from the AF under microscope. For rat NP cells isolation, the NP tissue obtained was digested for 30 min in a mixture of 0.4% Pronase (Roche Diagnostics, 10165921001) and 0.0125% collagenase P (Roche Diagnostics, 11213865001) [71]; for human NP cells isolation, the NP tissue obtained was digested for 30 min in 0.0125% collagenase P (Roche Diagnostics, 11213865001) [72]. The digested tissue was then passed through a cell strainer (BD Falcon, 352360) with a pore size of 100  $\mu$ m and was washed 3 times with phosphate-buffered saline (PBS; Gibco, 20012027). The isolated cells were maintained in Dulbecco's Modified Eagle Medium/Nutrient Mixture F-12 (DMEM/F-12; Gibco, 11320033) containing 10% fetal bovine serum (FBS; Gibco 10099141C), supplemented with 1% penicillin-streptomycin combination (Gibco, 15070063) at 37°C in a humidified atmosphere of 5% CO<sub>2</sub>.

Passage 1 and 2 was used in this study. For in vitro compression model, the cells were placed in a compression apparatus as previously described [27,42,73].

### Rat AF cell line culture

Rat AF cell line was a gift from Prof. Di Chen from University of Chinese Academy of Sciences and was maintained in DMEM/F-12 containing 10% FBS, supplemented with 1% penicillin-streptomycin combination at 37°C in a humidified atmosphere of 5% CO<sub>2</sub>.

### in vitro siRNA and adenovirus transfection

The siRNA duplexes targeting rat *Krt8*, *Krt18*, *Krt19*, *Plk4*, *Tbk1*, *Pkn1*, *Pkn2*, *Srpk1*, *Ttbk2* was designed and synthesized by Tsingke (China). siRNA sequences used in this study were listed in Table S1. The knockdown efficiency, in both mRNA and protein level was evaluated and the off-target effects of siRNA was excluded by confirming the consistence of results using at least 2 different and effective pairs of siRNAs in all knockdown experiments. siRNA transfection was performed using Lipofectamine RNAiMAX Reagent (Invitrogen, 13778) according to the manufacturer's instructions. Briefly, rat primary NP cells in passage 1 or 2 were seeded in a 6-well plate, after adhesion, incubated the cells with Optic-MEM medium (Thermo, 31985062) at 37°C for 2 h. Cells were then transfected with 100 nM siRNA or

NC (negative control, scramble sequence) siRNA using Lipofectamine RNAiMAX, incubated at 37°C for 6 h. Finally, cells were washed with PBS and changed the medium with completed culture medium. The cells were then subjected to in vitro compression after 24 h.

The adenovirus for overexpression of rat wildtype *Krt8*, *Krt18*, *Krt19* and mutant *Krt8* S27D, S35D, S36D, S43D, S51D, T305D was manufactured by Hanbio (China). The transfection was performed according to the manufacturer's instructions. Briefly, rat primary NP cells in passage 1 or 2 were seeded in a 6-well plate, after adhesion, the adenovirus was added to the culture medium (multiplicity of infection = 30), incubated at 37°C for 12 hours. Finally, cells were washed with PBS and changed the medium with completed culture medium. The cells were then subjected to in vitro compression after 48 h.

### **Protein extraction, co-immunoprecipitation (co-IP), and western blot analysis**

NP cells, AF cells, or rat coccygeal NP tissue were harvested and lysed in radioimmune precipitation assay (RIPA) buffer (Beyotime, P0013) containing a complete protease inhibitor cocktail and phosphatase inhibitor cocktail (Roche Diagnostics, 5892791001, 4906845001), and the concentrations of protein were determined by Pierce BAC Protein Assay Kit (Thermo, 23225). Protein isolation kits (Solarbio, E×1260, E×1240) were used for protein isolation from endoplasmic reticulum or Golgi apparatus.

Co-IP experiments were performed to verify the binding between proteins of interest in NP cells. The co-IP complexes were purified by Millipore Sigma PureProteome Protein A/G Mix Magnetic Bead System (LSKAGAG10, Fisher Scientific). The proteins were harvested and analyzed by western blot analysis. The antibodies against ACAN/aggrecan (AB1031), p-Ser/Thr (05–368) were purchased from Millipore, MMP3 (17873), GAPDH (60004–1) were purchased from Proteintech, and KRT8 (ab53280), IL6 (ab9324), LC3B (ab48394), SQSTM1 (ab109012), and p-PKN1 and 2 (ab187660) were purchased from Abcam; cleaved-CASP3/caspase 3 (Asp175; TA7022) was purchased from ab-mart; RAB33B (PA5–104074) was purchased from Thermo Scientific; ATG16L1 (8089) was purchased from Cell Signaling Technology; GOLGA2/GM130 (A16248), PKN1 (A0553), and PKN2 (A19746) were purchased from Abclonal; CANX/calnexin (sc -23,954) was purchased from Santa Cruz Biotechnology.

Proteins were separated by electrophoresis, followed by transferring to PVDF membranes (Merck Millipore, ISEQ08100). Blots were blocked with 5% bovine serum albumin (BSA; Solarbio, A8010), probed with primary antibodies at 4°C overnight, followed by incubation of appropriate secondary antibodies at room temperature (RT) for 2 h. Finally, the PVDF membranes were detected using Immobilon Western Chemiluminescent HRP Substrate (Millipore Corporation, WBKLS0100) and observed under Amersham Imager 600 (General Electric.).

### **RNA extraction and qPCR analysis**

Total RNA of NP cells or rat coccygeal NP tissues were harvested using MiniBEST Universal RNA Extraction Kit (TaKaRa, 9767) according to manufacturer's instructions. Reverse transcription was performed with PrimeScript RT Master Mix (TaKaRa, RR036A). Synthesized cDNA was then subjected to qPCR analysis using TB Green Premix Ex Taq II (TaKaRa, RR820A). The reactions were performed with CFX96 (Bio-Rad). Gene expression levels were reported as relative fold change, with *Gapdh* as an internal control. Primers sequences used in this study were shown in Table S2.

### **In vitro immunofluorescence staining**

NP cells were fixed in freshly prepared 4% paraformaldehyde (PFA; Solarbio, P1110) for 30 min, permeabilized by 0.1% Triton X-100 (Beyotime, P0096) for 30 min. Then the cells were and blocked by 1% BSA in PBS for 1 h, incubated with primary antibody at 4°C overnight, with appropriate secondary antibodies at RT for 2 h and with DAPI (C1006, Beyotime) at RT for 10 min. Finally, the cells were analyzed under a fluorescence microscope (BX53, OLYMPUS). Antibody against KRT8 (ab53280) and LC3B (ab48394) were purchased from Abcam.

### **Histology and immunofluorescence staining for disc sections**

Mouse L4–5 discs, Cy7–8 discs, or rat Cy7–8 discs were harvested, fixed in 4% freshly prepared PFA for 48 h, decalcified for 8 weeks with 10% EDTA at RT under gentle shaking, then dehydrated, paraffin-embedded, and sectioned at 5 µm. The sections were deparaffinized by xylene, rehydrated by ethanol. The hematoxylin-eosin (HE) staining kit (Solarbio, G1120) or safranin O-fast green (SOFG) staining kit (Solarbio, G1371) were used according to the manufactures' instructions, and the sections were graded by a previously published method [16,74]. For the IF staining, citrate buffer (0.1 mol/L, pH 6.0) was used to perform antigen-retrieval on deparaffinized and dehydrated sections. After blocking in 10% normal goat serum (Solarbio, SL038) at RT for 1 h, the sections were then incubated with primary antibody at 4°C over-nights, with appropriate secondary antibodies at RT for 2 h and with DAPI (Beyotime, C1006) for 10 min. Finally, the sections were analyzed under a fluorescence microscope (BX53, OLYMPUS). Fluorescence intensity was quantified using ImageJ (National Institutes of Health) software. The antibody against ACAN/aggrecan (AB1031) was purchased from Millipore, MMP3 (17873) was purchased from Proteintech, and KRT8 (ab53280) was purchased from Abcam.

### **Micro-CT, X-ray, and MRI analysis**

Mice and rats were treated as indicated. Before radiology evaluation, mice and rats were euthanized by inhaling an



excessive amount of isoflurane. Lateral radiographs were taken (exposure time, 0.06 s; distance, 100 cm; current, 160 mA; voltage, 50 kV) using the DRX-Ascend system (Carestream). Prone-position MRI was performed using a 3.0 T system (GE) to obtain T2-weighted images (repetition time, 1600 ms; echo time, 85 ms; field of view, 80 × 80 mm; slice thickness, 2.0 mm). Micro-CT was performed by the high-resolution micro-CT scanner (Bruker, Skyscan1276), for quantitative disc height evaluation. The modified Pfirrmann grading system was employed to evaluate the degree of disc degeneration by MRI scan [70]. The disc height index (DHI) was calculated as previously described [75], and the DHI percentage (DHI%) was calculated as  $DHI \text{ of Cy7-8} \div DHI \text{ of Cy8-9}$ .

### Apoptosis assay

For in vitro cell experiments, NP cells were harvested in 0.25% trypsin (Solarbio, T1350) and washed three times with cold PBS. The apoptosis of NP cells was evaluated by ANXA5/propidium iodide (PI) apoptosis detection kit (BD Biosciences, 556547) by flow cytometry. For disc sections, terminal deoxynucleotidyl transferase dUTP nick end labeling (TUNEL) assay was performed using In Situ Cell Death Detection Kit (Roche Diagnostics, 11684795910) according to manufacturer's instructions.

### Animal disc degeneration model establishment and AAV, shRNA transfection in vivo

Mouse lumbar instability model (LSI) [40] and mouse tail suturing compressive model (TCS) [41] was established as previously described. Briefly, male mice of 8 weeks of age (skeletally mature) were anesthetized with isoflurane, and the surgical area was sterilized with 70% ethanol. For LSI surgery, the 3<sup>rd</sup>–5<sup>th</sup> lumbar (L3–L5) spinous processes along with the supraspinous and interspinous ligaments were resected to induce instability of lumbar spine. Sham operations were carried out only by detaching of the posterior paravertebral muscles from the L3–L5 vertebrae. For TCS surgery, the IVD between the 7th coccygeal vertebra (Cy7) and the 8th coccygeal vertebra (Cy8) was localized via X-ray. Two parallel lines 2 mm apart around the tail were made, and the skin was cut along these parallel lines. A 2-mm-wide skin was then cut from the tail. Finally, a 4–0 silk thread was used to sew the skin and subcutaneous tissue via a simple end-to-end suture to put the broken skin closed together. The sham group was just removal of a 2-mm-wide skin patch without compressive suture. Cy8–9 IVD, which is one disc away from the compressed disc, was chosen as the control.

Rat tail compression-induced IDD model (TCM) was established as previously described [42]. Briefly, rats of 8 weeks of age (skeletally mature) were anesthetized with isoflurane, and the surgical area was sterilized with 70% ethanol. The compression-loading apparatus were instrumented on the Cy7 and Cy9, resulting in a compression induce IDD in Cy7–8 and Cy8–9. The type 5 adeno-associated virus (AAV5) (2  $\mu$ l,  $2 \times 10^{13}$  VG/ml) or shRNA (20 pmol) was directly injected to the NP of the tail discs by a 33-gauge needle (Hamilton).

### mRNA sequencing and bioinformatic analysis

The mRNA sequencing was provided by Genedenovo Biotechnology Co., Ltd (Guangzhou, China). Briefly, Total RNA of the NP cells was extracted using Trizol reagent (Invitrogen, 15596026) according to the manufacturer's protocol. The mRNA was then enriched, fragmented, and reversely transcribed into cDNA. The resulting cDNA library was sequenced using Illumina Novaseq6000 by Gene Denovo Biotechnology Co. (Guangzhou, China). Differentially expressed genes (DEGs) were identified using the DESeq2 package ( $|\text{fold change}| \geq 1.5$ ,  $P < 0.05$ ). Gene Ontology (GO) enrichment analysis was performed, and the results visualized with the OmicShare tool, an online platform for data analysis ([https://www.omicshare.com/tools/Home/Soft/enrich\\_circle](https://www.omicshare.com/tools/Home/Soft/enrich_circle)). Gene set enrichment analysis (GSEA) was performed with GSEA 4.1.0 software (Broad Institute).

### Quantitative phosphoproteomic analysis, kinase prediction and phosphorylation site – specific antibody generation

The NP tissues were harvested from the TCM rats, and the NP tissues from Cy7–8 and Cy8–9 IVDs were defined as the compression group, and the NP tissues from Cy6–7 and Cy9–10 IVDs were defined as the control group ( $n = 3$ ). 4D label-free quantitative phosphoproteomic analysis was then provided by PTM – BIOLAB (China).

Group-based Prediction System (GPS) V5.0 software [53] was employed to predict the protein kinase based on the motifs surrounding the phosphorylated site.

The polyclonal phosphorylation site – specific antibody targeting rat p-Ser43 KRT8 was generated, based on peptide “FSRVG-(p-S)-SSS” by ABclonal Technology.

### Statistical analysis

Trial experiments or experiments performed previously were used to determine sample size with adequate statistical power. The investigator was blinded to the group allocation and during the experiment. Data are presented as mean  $\pm$  SD in all experiments. An independent experiment was performed by a batch of primary cells harvested from a single subject (a single rat or a single human sample in each independent experiment, not a replicate from a same donors). All statistical analyses were performed with GraphPad Prism 9 (GraphPad Software Inc, USA). An *F*-test for equality of variances was performed to ensure the same variance of tested groups. The *Shapiro-Wilk test* or *D'Agostino test* was performed to determine whether the collected data follows a normal distribution. Data were analyzed by the Student's unpaired t test to compare means when there were 2 experimental groups, by one-way ANOVA with the Tukey post hoc test to compare means among >2 groups, and by two-way ANOVA with the Tukey post hoc test when there were 2 independent variables. Here,  $n$  refers to the number of independent experiments or mice per group. Significance was defined as  $p < 0.05$ .

## Disclosure statement

No potential conflict of interest was reported by the authors.

## Funding

This work was supported by the National Natural Science Foundation of China (82020108019, 81730065, 82130070, 82002347), Innovation Team Projects – Innovation Capability Support Program of Shaanxi Province (2020TD-036) and Key Industrial Chain Program of Shaanxi (2022ZDLSF02-12)

## Availability of data and materials

Data collected and analyzed for the study are available from the corresponding authors upon reasonable request.

## Consent for publication

Written informed consent was obtained from each participant.

## Ethics approval and consent to participate

Ethical approval of the current study was obtained from the Institutional Review Board of Xijing Hospital of the Fourth Military Medical University (KY20203146–1). All animal experiments were approved by the Animal Use and Care Committee of the Air Force Medical University and conducted in accordance with the National Institute for Health Guide for the Care and Use of Laboratory Animals.

## ORCID

Di Wang  <http://orcid.org/0000-0001-5036-7909>

Qiliang Shang  <http://orcid.org/0000-0003-3689-2373>

## References

- [1] Hoy D, March L, Brooks P, et al. The global burden of low back pain: estimates from the global burden of disease 2010 study. *Ann Rheum Dis*. 2014;73:968–974.
- [2] Gianola S, Bargeri S, Del Castillo G, et al. Effectiveness of treatments for acute and subacute mechanical non-specific low back pain: a systematic review with network meta-analysis. *Br J Sports Med*. 2022;56:41–50.
- [3] Patrick N, Emanski E, Knaub MA. Acute and chronic low back pain. *Med Clin North Am*. 2014;98:777–89, xii.
- [4] Knezevic NN, Candido KD, Vlaeyen JWS, et al. Low back pain. *Lancet*. 2021;398:78–92.
- [5] de Schepper EI, Damen J, van Meurs JB, et al. The association between lumbar disc degeneration and low back pain: the influence of age, gender, and individual radiographic features. *Spine (Phila Pa 1976)*. 2010;35:531–536.
- [6] Adams MA, Dolan P. Spine biomechanics. *J Biomech*. 2005;38:1972–1983.
- [7] Hartman RA, Yurube T, Ngo K, et al. Biological responses to flexion/extension in spinal segments ex-vivo. *J Orthop Res*. 2015;33:1255–1264.
- [8] Adams MA, Freeman BJ, Morrison HP, et al. Mechanical initiation of intervertebral disc degeneration. *Spine (Phila Pa 1976)*. 2000;25:1625–1636.
- [9] Humzah MD, Soames RW. Human intervertebral disc: structure and function. *Anat Rec*. 1988;220:337–356.
- [10] Yurube T, Han I, Sakai D. Concepts of regeneration for spinal diseases in 2022. *Int J Mol Sci*. 2022;23:9710.
- [11] Risbud MV, Shapiro IM. Role of cytokines in intervertebral disc degeneration: pain and disc content. *Nat Rev Rheumatol*. 2014;10:44–56.
- [12] Adams MA, Roughley PJ. What is intervertebral disc degeneration, and what causes it? *Spine (Phila Pa 1976)*. 2006;31:2151–2161.
- [13] Park EH, Moon SW, Suh HR, et al. Disc degeneration induces a mechano-sensitization of disc afferent nerve fibers that associates with low back pain. *Osteoarthritis Cartilage*. 2019;27:1608–1617.
- [14] Yurube T, Takada T, Suzuki T, et al. Rat tail static compression model mimics extracellular matrix metabolic imbalances of matrix metalloproteinases, aggrecanases, and tissue inhibitors of metalloproteinases in intervertebral disc degeneration. *Arthritis Res Ther*. 2012;14:R51.
- [15] Yurube T, Nishida K, Suzuki T, et al. Matrix metalloproteinase (MMP)-3 gene up-regulation in a rat tail compression loading-induced disc degeneration model. *J Orthop Res*. 2010;28:1026–1032.
- [16] Chen S, Wu X, Lai Y, et al. Kindlin-2 inhibits Nlrp3 inflammatory activation in nucleus pulposus to maintain homeostasis of the intervertebral disc. *Bone Res*. 2022;10:5.
- [17] He R, Wang Z, Cui M, et al. HIF1A alleviates compression-induced apoptosis of nucleus pulposus derived stem cells via upregulating autophagy. *Autophagy*. 2021;17:1–23.
- [18] Yurube T, Hirata H, Ito M, et al. Involvement of Autophagy in Rat tail static compression-induced intervertebral disc degeneration and notochordal cell disappearance. *Int J Mol Sci*. 2021;22:22.
- [19] Yurube T, Hirata H, Kakutani K, et al. Notochordal cell disappearance and modes of apoptotic cell death in a rat tail static compression-induced disc degeneration model. *Arthritis Res Ther*. 2014;16:R31.
- [20] Jacob JT, Coulombe PA, Kwan R, et al. Types I and II keratin intermediate filaments. *Cold Spring Harb Perspect Biol*. 2018;10:10.
- [21] Mohanty S, Pinelli R, Pricop P, et al. Chondrocyte-like nested cells in the aged intervertebral disc are late-stage nucleus pulposus cells. *Aging Cell*. 2019;18:e13006.
- [22] Choi KS, Cohn MJ, Harfe BD. Identification of nucleus pulposus precursor cells and notochordal remnants in the mouse: implications for disk degeneration and chordoma formation. *Dev Dyn*. 2008;237:3953–3958.
- [23] Tessier S, Risbud MV. Understanding embryonic development for cell-based therapies of intervertebral disc degeneration: toward an effort to treat disc degeneration subphenotypes. *Dev Dyn*. 2021;250:302–317.
- [24] Gan Y, He J, Zhu J, et al. Spatially defined single-cell transcriptional profiling characterizes diverse chondrocyte subtypes and nucleus pulposus progenitors in human intervertebral discs. *Bone Res*. 2021;9:37.
- [25] Sun Z, Wang HQ, Liu ZH, et al. Down-regulated CK8 expression in human intervertebral disc degeneration. *Int J Med Sci*. 2013;10:948–956.
- [26] Tam V, Chen P, Yee A, et al. DIPPER, a spatiotemporal proteomics atlas of human intervertebral discs for exploring ageing and degeneration dynamics. *Elife*. 2020;9. doi:10.7554/eLife.64940.
- [27] Sun Z, Guo YS, Yan SJ, et al. CK8 phosphorylation induced by compressive loads underlies the downregulation of CK8 in human disc degeneration by activating protein kinase C. *Lab Invest*. 2013;93:1323–1330.
- [28] Klionsky DJ, Abdelmohsen K, Abe A, et al. Guidelines for the use and interpretation of assays for monitoring autophagy. 3rd ed. Vol. 12, *Autophagy*; 2016. p. 1–222.
- [29] Ao X, Zou L, Wu Y. Regulation of autophagy by the Rab GTPase network. *Cell Death & Differentiation*. 2014;21:348–358.
- [30] Hurley JH, Young LN. Mechanisms of Autophagy initiation. *Annu Rev Biochem*. 2017;86:225–244.
- [31] Yurube T, Buchser WJ, Moon HJ, et al. Serum and nutrient deprivation increase autophagic flux in intervertebral disc annulus fibrosus cells: an in vitro experimental study. *Eur Spine J*. 2019;28:993–1004.

- [32] Yurube T, Ito M, Kakiuchi Y, et al. Autophagy and mTOR signaling during intervertebral disc aging and degeneration. *JOR Spine*. 2020;3:e1082.
- [33] Tsujimoto R, Yurube T, Takeoka Y, et al. Involvement of autophagy in the maintenance of rat intervertebral disc homeostasis: an in-vitro and in-vivo RNA interference study of Atg5. *Osteoarthritis Cartilage*. 2022;30:481–493.
- [34] Ito M, Yurube T, Kanda Y, et al. Inhibition of Autophagy at different stages by ATG5 knockdown and chloroquine supplementation enhances consistent human disc cellular apoptosis and senescence induction rather than extracellular matrix catabolism. *Int J Mol Sci*. 2021;22:3965.
- [35] Wang D, Zhang P, Xu X, et al. Knockdown of cytokeratin 8 overcomes chemoresistance of chordoma cells by aggravating endoplasmic reticulum stress through PERK/elf2 $\alpha$  arm of unfolded protein response and blocking autophagy. *Cell Death Dis*. 2019;10(12):887. DOI:10.1038/s41419-019-2125-9
- [36] Baek A, Son S, Baek YM, et al. KRT8 (keratin 8) attenuates necrotic cell death by facilitating mitochondrial fission-mediated mitophagy through interaction with PLEC (plectin). *Autophagy*. 2021;17:3939–3956.
- [37] Baek A, Yoon S, Kim J, et al. Autophagy and KRT8/keratin 8 protect degeneration of retinal pigment epithelium under oxidative stress. *Autophagy*. 2017;13:248–263.
- [38] Ito M, Yurube T, Kakutani K, et al. Selective interference of mTORC1/RAPTOR protects against human disc cellular apoptosis, senescence, and extracellular matrix catabolism with Akt and autophagy induction. *Osteoarthritis Cartilage*. 2017;25:2134–2146.
- [39] Gao B, Yin J, Xu X, et al. Leptin receptor-expressing cells represent a distinct subpopulation of notochord-derived cells and are essential for disc homeostasis. *J Orthop Translat*. 2020;21:91–99.
- [40] Oichi T, Taniguchi Y, Soma K, et al. A mouse intervertebral disc degeneration model by surgically induced instability. *Spine (Phila Pa 1976)*. 2018;43:E557–564.
- [41] Liu Z, Zhou Q, Zheng J, et al. A novel in vivo mouse intervertebral disc degeneration model induced by compressive suture. *Exp Cell Res*. 2021;398:112359.
- [42] Wang D, Peng P, Dudek M, et al. Restoring the dampened expression of the core clock molecule BMAL1 protects against compression-induced intervertebral disc degeneration. *Bone Res*. 2022;10:20.
- [43] Lahdeniemi IAK, Misiorek JO, Antila CJM, et al. Keratins regulate colonic epithelial cell differentiation through the Notch1 signaling pathway. *Cell Death & Differentiation*. 2017;24:984–996.
- [44] Choi H, Merceron C, Mangiavini L, et al. Hypoxia promotes noncanonical autophagy in nucleus pulposus cells independent of MTOR and HIF1A signaling. *Autophagy*. 2016;12:1631–1646.
- [45] Itoh T, Fujita N, Kanno E, et al. Golgi-resident small GTPase Rab33B interacts with Atg16L and modulates autophagosome formation. *Mol Biol Cell*. 2008;19:2916–2925.
- [46] Pantoom S, Konstantinidis G, Voss S, et al. RAB33B recruits the ATG16L1 complex to the phagophore via a noncanonical RAB binding protein. *Autophagy*. 2021;17:2290–2304.
- [47] Dudley LJ, Cabodevilla AG, Makar AN, et al. Intrinsic lipid binding activity of ATG16L1 supports efficient membrane anchoring and autophagy. *Embo J*. 2019;38:e100554.
- [48] Ku NO, Omary MB. A disease- and phosphorylation-related non-mechanical function for keratin 8. *J Cell Biol*. 2006;174:115–125.
- [49] Roux A, Loranger A, Lavoie JN, et al. Keratin 8/18 regulation of insulin receptor signaling and trafficking in hepatocytes through a concerted phosphoinositide-dependent Akt and Rab5 modulation. *Faseb J*. 2017;31:3555–3573.
- [50] Son S, Baek A, Lee JH, et al. Autophagosome-lysosome fusion is facilitated by plectin-stabilized actin and keratin 8 during macroautophagic process. *Cell Mol Life Sci*. 2022;79:95.
- [51] Snider NT, Omary MB. Assays for posttranslational modifications of intermediate filament proteins. *Methods Enzymol*. 2016;568:113–138.
- [52] Snider NT, Omary MB. Post-translational modifications of intermediate filament proteins: mechanisms and functions. *Nat Rev Mol Cell Biol*. 2014;15:163–177.
- [53] Wang C, Xu H, Lin S, et al. GPS 5.0: an update on the prediction of kinase-specific phosphorylation sites in proteins. *Genomics Proteomics Bioinf*. 2020;18:72–80.
- [54] Watanabe G, Saito Y, Madaule P, et al. Protein kinase N (PKN) and PKN-related protein rhophilin as targets of small GTPase Rho. *Science*. 1996;271:645–648.
- [55] Schofield P. Assessment and management of pain in older adults with dementia: a review of current practice and future directions. *Curr Opin Support Palliat Care*. 2008;2:128–132.
- [56] Stokes IA, Iatridis JC. Mechanical conditions that accelerate intervertebral disc degeneration: overload versus immobilization. *Spine (Phila Pa 1976)*. 2004;29:2724–2732.
- [57] Qu H, Yu LJ, Wu JT, et al. Spine system changes in soldiers after load carriage training in a plateau environment: a prediction model research. *Mil Med Res*. 2020;7:63.
- [58] Toivola DM, Boor P, Alam C, et al. Keratins in health and disease. *Curr Opin Cell Biol*. 2015;32:73–81.
- [59] Jin YJ, Chennupati R, Li R, et al. Protein kinase N2 mediates flow-induced endothelial NOS activation and vascular tone regulation. *J Clin Invest*. 2021;131(21):e145734.
- [60] Sakaguchi T, Takefuji M, Wettschureck N, et al. Protein kinase N promotes stress-induced cardiac dysfunction through phosphorylation of myocardin-related transcription factor a and disruption of its interaction with actin. *Circulation*. 2019;140:1737–1752.
- [61] Roh EJ, Darai A, Kyung JW, et al. Genetic therapy for intervertebral disc degeneration. *Int J Mol Sci*. 2021;22(4):1579.
- [62] Zehra U, Tryfonidou M, Iatridis JC, et al. Mechanisms and clinical implications of intervertebral disc calcification. *Nat Rev Rheumatol*. 2022;18:352–362.
- [63] Bibby SR, Jones DA, Ripley RM, et al. Metabolism of the intervertebral disc: effects of low levels of oxygen, glucose, and pH on rates of energy metabolism of bovine nucleus pulposus cells. *Spine (Phila Pa 1976)*. 2005;30:487–496.
- [64] Wang D, He X, Wang D, et al. Quercetin suppresses apoptosis and attenuates intervertebral disc degeneration via the SIRT1-autophagy pathway. *Front Cell Dev Biol*. 2020;8:613006.
- [65] Zuela-Sopilniak N, Lammerding J. Can't handle the stress? Mechanobiology and disease. *Trends Mol Med*. 2022;28:710–725.
- [66] Levy Nogueira M, da Veiga Moreira J, Baronzio GF, et al. Mechanical stress as the common denominator between chronic inflammation, cancer, and Alzheimer's disease. *Front Oncol*. 2015;5:197.
- [67] Vergroesen PP, Kingma I, Emanuel KS, et al. Mechanics and biology in intervertebral disc degeneration: a vicious circle. *Osteoarthritis Cartilage*. 2015;23:1057–1070.
- [68] Tschumperlin DJ, Lagares D. Mechano-therapeutics: targeting mechanical signaling in fibrosis and tumor stroma. *Pharmacol Ther*. 2020;212:107575.
- [69] Rocha DN, Carvalho ED, Relvas JB, et al. Mechanotransduction: exploring new therapeutic avenues in central nervous system pathology. *Front Neurosci*. 2022;16:861613.
- [70] Pfirmann CW, Metzdorf A, Zanetti M, et al. Magnetic resonance classification of lumbar intervertebral disc degeneration. *Spine (Phila Pa 1976)*. 2001;26:1873–1878.
- [71] Hiyama A, Sakai D, Risbud MV, et al. Enhancement of intervertebral disc cell senescence by WNT/beta-catenin signaling-induced matrix metalloproteinase expression. *Arthritis Rheum*. 2010;62:3036–3047.
- [72] Lee JT, Cheung KM, Leung VY. Systematic study of cell isolation from bovine nucleus pulposus: improving cell yield and experimental reliability. *J Orthop Res*. 2015;33:1743–1755.
- [73] Peng P, Wang D, Xu X, et al. Targeting clock-controlled gene Nrf2 ameliorates inflammation-induced intervertebral disc degeneration. *Arthritis Res Ther*. 2022;24:181.
- [74] Tam V, Chan WCW, Leung VYL, et al. Histological and reference system for the analysis of mouse intervertebral disc. *J Orthop Res*. 2018;36:233–243.
- [75] Han B, Zhu K, Li FC, et al. A simple disc degeneration model induced by percutaneous needle puncture in the rat tail. *Spine (Phila Pa 1976)*. 2008;33:1925–1934.